SIMULTANEOUS MEASUREMENT OF ISOTOPE-FREE TRACER AND INTERDIFFUSION COEFFICIENTS IN SANDWHICH TYPE DIFFUSION COUPLES

by

ESIN AKBULUT SCHULZ
B.S. Istanbul Technical University, 2003
M.S. Istanbul Technical University, 2006
M.S. University of Central Florida, 2015

A dissertation submitted in partial fulfillment of the requirements
for the degree of Doctor of Philosophy
in the Department of Materials Science and Engineering
in the College of Engineering and Computer Science
at the University of Central Florida
Orlando, Florida

Fall Term
2018

Major Professor: Yongho Sohn

ABSTRACT

The experimental determination of the tracer or self-diffusion coefficient as a function of composition can be quite burdensome in alloys since separate measurements must be carried out for each alloy composition. A new formalism recently developed by I.V. Belova, N.S. Kulkarni, Y.H. Sohn and G.E. Murch, based on linear response theory combined with the Boltzmann–Matano method allows determination of tracer and interdiffusion coefficients simultaneously from a single, isotope-free solid to solid diffusion couple experiment. In this study, for the first time, an experimental investigation with an analytical approach based on the new formalism has been carried out in the binary Cu-Ni system. Pure Cu and Ni thin films were deposited in between several binary diffusion couples with varying terminal alloy compositions (such as Cu, Cu-25Ni, Cu-50Ni, Cu-75Ni, Ni). Diffusion couples were then annealed at 800°C, 900°C and 1000°C. After annealing, the couples were water quenched, cross-sectioned, and prepared for compositional characterization. Scanning Electron Microscopy was employed to examine the interdiffusion zone. Energy Dispersive X-ray Spectroscopy was conducted to obtain concentration profiles for quantitative analysis. The superposition of the concentration profiles of thin film and interdiffusion were analyzed for the simultaneous determination of tracer and interdiffusion coefficients. The tracer diffusion coefficient D_{Cu}^{*} , D_{Ni}^{*} and inter-diffusion coefficients simultaneously determined using the experimental methodology based on the novel formalism derived, and produced results consistent with previously reported values determined independently by radiotracer and interdiffusion experiments.

The author would like to dedicate this work to her family that have supported her throughout the years that have led up to this milestone

ACKNOWLEDGMENTS

I write this acknowledgement with the deepest gratitude for all the people who have given me the opportunity to earn my Ph.D. in Materials Science and Engineering.

First and foremost, I would like to express my sincere gratitude to my advisor Dr. Yongho Sohn for the generosity and scholarship he provided, for his patience and support during this time.

Besides my advisor, I would like to thank the rest of my committee members Dr. K. Coffey, Dr. S. Florczyk, Dr. Y. Bai, and Dr. N. Orlovskaya for their insightful comments and encouragements.

I thank my fellow labmates for the stimulating discussions, for the sleepless nights we were working together before deadlines, and for all the fun we have had in the last couple of years.

Last but not the least, I would like to thank to my family and friends for all your patience, love and support. My life is a journey that has come with ups and downs but I have reached my destination and it's all worth the pain.

"The task ahead of you is never greater than the strength within you."

TABLE OF CONTENTS

LIST OF FIGURES

LIST OF TABLES

LIST OF ACRONYMS

γ_A	Activity Coefficient
t	Anneal Time
λ	Boltzmann Variable
CALPHAD	Calculation of Phase Diagrams
μ_A	Chemical Potential
C_i	Concentration of component i
f	Correlation Factor
F_A	Correlation Function of A atoms
DICTRA	Diffusion controlled Transformation
FIB	Focused Ion Beam
J_i	Flux of Component i
HEA	High Entropy Alloy
$\widetilde{D}$	Interdiffusion Coefficient

D_i	Intrinsic Diffusion Coefficient
v	Lattice Drift
x_o	Matano Plane Position
X_A	Mole Fraction of A
N	Number of Lattice Sites
L_{ij}	Onsager's Phenomenological Coefficient
x	Position
SEM	Scanning Electron Microscope
D_s	Self Diffusion Coefficient
SIMS	Secondary Ion Mass Spectrometer
T	Temperature
S	Thermodynamic Factor
X_i	Thermodynamic Forces
D_A^*	Tracer Diffusion Coefficient

UHV	Ultra High Vacuum
∅	Vacancy wind effect
XEDS	X-Ray Energy Dispersive Spectroscopy

CHAPTER 1 INTRODUCTION

Diffusional studies have been fundamental in the materials science due to its direct correlation to microstructural changes in solids. Since diffusion largely control the overall properties of a material, understanding of the diffusion behavior of components in any given system is essential. To achieve this understanding, scientists were obligated to define the diffusion process and express in mathematical equations. As diffusion studies conducted over the years, various diffusion coefficients were introduced (e.g, tracer diffusion, inter-diffusion, intrinsic diffusion). There are several relationships developed between the types of diffusion coefficients. For instance, in a binary system, the interdiffusion coefficient can be related to tracer diffusion coefficients through Darken-Manning equation [1]. Similarly, the interdiffusion coefficient can be related to the intrinsic diffusion coefficients [2].

Given that most alloys in practical use are multicomponent, when modeling microstructural evaluations in multicomponent alloys, which kinetic parameter to utilize and how these parameters could be obtained becomes imperative. For instance, in order to solve the interdiffusion equations for an alloy composed of n number of component, minimum of (n-1) diffusion couples would be necessary and their diffusion path must intercept at the same composition. The probability of intersecting three diffusion paths in Gibbs tetrahedron is infinitely small. Furthermore, physical interpretation of interdiffusion coefficients in multicomponent alloys becomes quite complex. Therefore, tracer diffusion data is more suitable

kinetic data for construct mobility diffusion database and alloy modeling. However, an efficient way of obtaining tracer diffusion coefficient is necessary.

Primary experiments for calculating interdiffusion coefficients are called diffusion couple experiments where two alloys or pure materials are brought in contact and annealed at high temperature to allow intermixing of components. Interdiffusion couple experiments are the most common and convenient way of measuring composition-dependent diffusion coefficients. It would be highly desirable to obtain accurate tracer diffusion coefficients from the traditional diffusion couple experiments without the use of radiotracers or stable isotopes.

The intrinsic diffusion coefficient determination involves intricate experiments that require inert marker displacement measurement. Out of all types of diffusion coefficient calculations, the tracer diffusion experiments provide the most fundamental information about the number of jumps an atom makes between the lattice sites and are the foundation of mobility databases [3]. DICTRA (Diffusion Controlled TRAnsformation) is a software developed to predict microstructural evolutions that operates under CALPHAD (CALculation of PHase Diagrams) framework [4]. Important kinetic parameter, such as tracer diffusion coefficient is used as an input to model/simulate diffusion related phenomena for multicomponent alloys. Traditionally, tracer diffusion data have been obtained using the thin film techniques with radioactive isotopes. Nowadays, the usage of radioactive tracers for diffusion studies are less common due to cost and safety concerns. The more common technique to measure tracer diffusivity utilizes secondary ion mass spectroscopy (SIMS) where stable isotopes are deposited on the surface of the sample and annealed at the desired temperature for a certain time. The depth

profiles in the sample are then measured using SIMS [5]. Using either technique to experimentally determine the tracer diffusion coefficient in alloys can be burdensome and costly due to the use of isotopes and the number of experiments required to assess composition- and temperature-dependence. Therefore, an efficient way of obtaining tracer diffusion coefficients is highly sought after.

A new formalism recently developed by Belova *et* al [6], based on linear response theory combined with the Boltzmann–Matano method allows determination of tracer and interdiffusion coefficients simultaneously from a single, isotope-free sandwich-type diffusion experiment. In this study, an analytical implementation of this new formalism is carried out to simultaneously determine interdiffusion coefficients, and tracer diffusion coefficients in the Cu-Ni system. Cu and Ni thin films were deposited in between several binary diffusion couples with varying terminal alloy compositions (Cu, Cu-25Ni, Cu-50Ni, Cu-75Ni, Ni). Diffusion couples were annealed at 800°C, 900°C and 1000°C, and the superimposed concentration profiles of thin film and interdiffusion were analyzed for the simultaneous determination of tracer and interdiffusion coefficients. SEM/XEDS was employed to examine the interdiffusion zone and determine concentration profiles. Results were compared to existing literature data obtained independently by interdiffusion and radiotracer experiments, and demonstrated that the tracer and interdiffusion coefficients can be simultaneously determined successfully. Simultaneous measurement of tracer and interdiffusion coefficients would provide an efficient and consistent way to distinguish the kinetic (e.g., mobility) and thermodynamic (e.g., thermodynamic factor, Φ) influences on the overall diffusion process in metallic alloys, for example, through the Darken model. The Cu-Ni

system was chosen for this investigation to demonstrate the validity of the new analytical framework, because there are ample data on both tracer diffusion and interdiffusion in the literature.

The main objective of this dissertation to extract tracer diffusion coefficients from a set of experiment consisted of simple configurations of alloys based on newly developed formalism by Belova et al. Firstly, diffusion studies will help to demonstrate the applicability of the mathematical modeling and validate the analytical approach as an efficient way of measuring tracer diffusion coefficients. Secondly, fundamental data of diffusion coefficients can be calculated by analyzing the concentration profiles. For example, intrinsic diffusivities of constituents has been widely studied using inert markers for many metallic systems [7, 8]. However, effects of marker size, amount and distribution on diffusion behavior and Kirkendall voids development have not been examined. In this experimental study, various size and distribution of Al_2O_3 makers were also employed in solid-to-solid, Cu vs. Ni diffusion couples, and their effects on the development of Kirkendall voids, and determination of interdiffusion coefficients and intrinsic diffusion coefficients were studied. Thirdly, tracer and interdiffusion coefficients can be measured within single experiment for self-consistency. Lastly, if successfully validated, this study would create a huge potential for obtaining tracer diffusivities for the elements (constituent, not impurity) without stable radiotracer isotopes, such as Aluminium.

CHAPTER 2 LITERATURE REVIEW

2.1 Diffusion Equations

Diffusional processes best understood using a formalism that relates how the atoms move to the current condition of the system. There are two main approaches to describing diffusion processes which are the atomistic approach and the phenomenological approach. The atomistic approach describes the sequential jumping of individual atoms from one lattice site. The continuum approach assumes a continuum solid and does not assume a particular diffusion mechanism. The phenomenological approach can be used to analyze and predict microstructural and composition evolution in a material using phenomenological expressions of irreversible thermodynamics. In this study, the phenomenological approach was used for quantitative analysis of the diffusion couples. The phenomenological formalism defines fluxes as measures of motion and relates them to forces defined in terms of gradients of the properties of the system calculated from the current condition of the system [9]. The flux represents the number of particles crossing a unit area per unit time. For example, the concentration is expressed in terms of number of particles per cm^3, and the distance x is in cm. Therefore, the diffusion coefficient will have the units of cm^2/s when the unit time is in seconds. Generally, flow of particles occurs from high concentration to low concentration. The flux of component *i* is expressed as J_i.

2.2 The Various Diffusion Coefficients and Inter-relationships

2.2.1 Self and Tracer Diffusion Coefficient

Even in pure solid material, despite the lack of chemical gradient, atoms move from one lattice position to another due to thermal vibration. Since there is no driving force, jumps occur in a random manner. This phenomenon is called Self Diffusion. The movement of atoms resulted in random jumps can be detected using isotopes of the same element by tracing the isotope in the material. Isotopes have the same number of protons, but different number of neutrons. This means they only differ in mass. The chemical reactivity of an element is determined by number of electrons in the planetary systems of its individual atoms e.g. by atomic number and not by atomic mass, therefore the chemical reactivity of an element's different isotopes are almost identical [10]. However, the difference in number of neutrons makes isotopes suitable for labelling and tracing the movement so that it can be detected within the same element while chemically behaving identically to the unlabeled counterpart.

To study self-diffusion of an element A, a very thin layer of radioactive isotopes of A; namely A*, are deposited on a material A and exposed to an annealing temperature T for a certain time, t. The whole sample is then serially sectioned, and intensity of emitted ray is measured at different depths (Figure 1). The tracer diffusion coefficient, D_A^* , can be calculated from the slope, $-\frac{1}{4D_A^* t}$, of the plot obtained from the serial sectioning [11]. Nowadays, the usage of radioactive tracers for diffusion studies are less common due to cost and safety concerns.

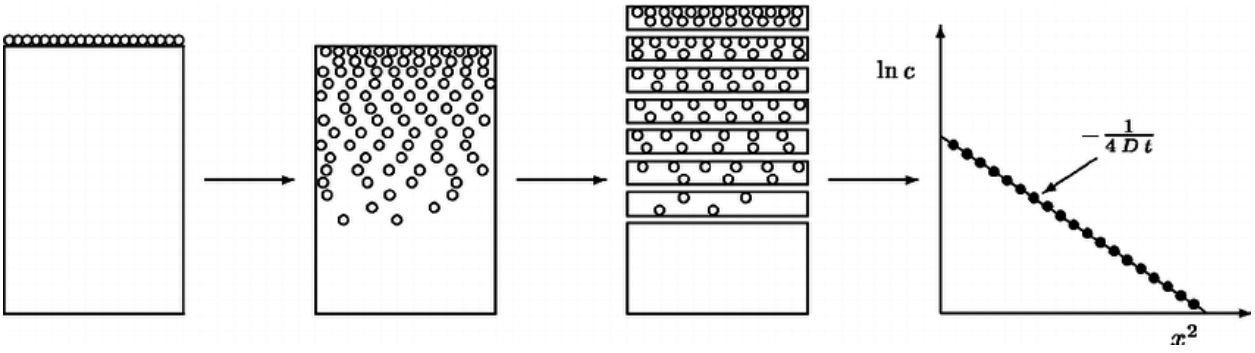

Figure 1 - Schematic illustration of traditional tracer method[12]

An alternative, and more common method to determine tracer diffusion, utilizes enriched stable isotopes rather than radioactive isotopes as tracers. In this method, secondary ion mass spectrometer's (SIMS) primary focused ion beam sputters off surface layers from the solid sample, simultaneously collecting and analyzing ejected secondary ions. Elemental composition as a function of depth is determined by a mass spectrometer measuring mass/charge ratio of the secondary ions [13]. SIMS is a powerful characterization tool not only because it can detect elements in the ppm to ppb range, but also it can distinguish different isotopes of the same element [14]. In order to determine the tracer diffusivity, a thin film of enriched stable isotopes is deposited on the surface of the sample via one of the deposition technique e.g. sputtering. Then the sample containing the deposited tracer film is annealed at the desired temperature for a certain time. The depth profiles in the sample are then measured using SIMS.

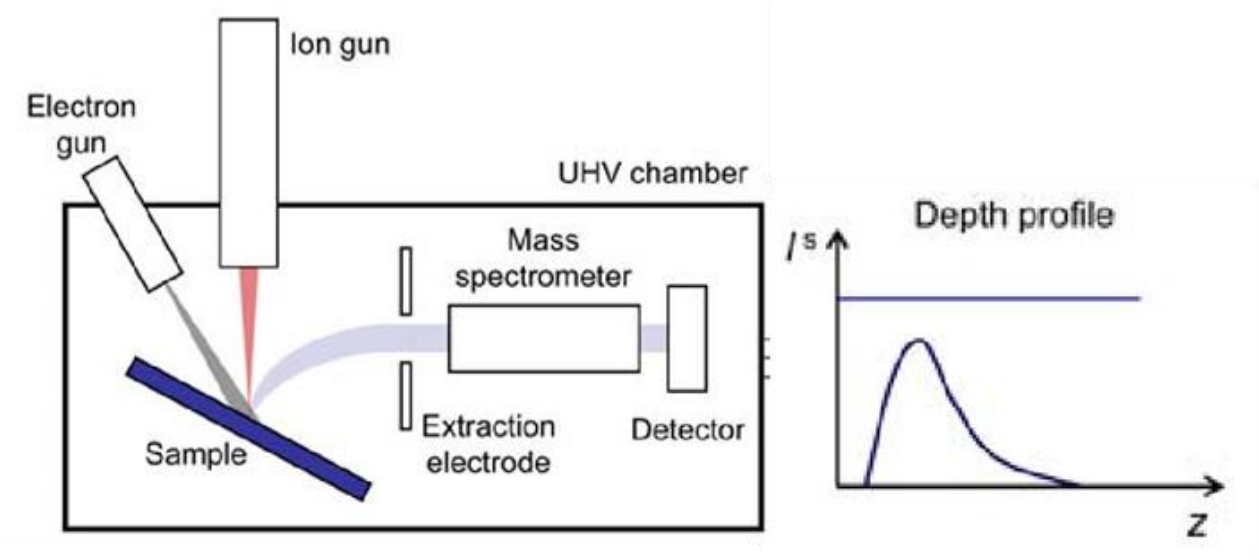

Figure 2 – Schematic diagram of SIMS equipment and depth profile[14]

The jumps of the tracer atoms are related to previous jumps and are not random. However, once tracer diffusivity is found, self-diffusivity can be calculated since they are related to each other by correlation factor, f [15]. In cubic system, this relationship is given by [11] [16].

$$D^* = fD_s \qquad (1)$$

where f is tracer correlation factor, D^* and D_s is tracer and self-diffusion coefficients, respectively.

2.2.2 Inter-diffusion and Intrinsic Diffusion

Intermixing of two constituents govern by diffusion equation and diffusion coefficient is a measure of how fast the intermixing is occurring. Adolf Fick was one of the first scientists

introduced the term diffusion coefficient and attempted to measure it [17]. His approach is now known as the continuum approach (also known as phenomenological approach) and is given by;

$$J_i = -D_i \frac{dC_i}{dx} \qquad (2)$$

Where J_i is the flux, D_i is diffusion coefficient, and $\frac{dC_i}{dx}$ is the gradient in the concentration of component *i* and it is applicable where there is no change in composition over time (steady state). The minus sign refers that typically atoms have tendency to move from high concentration to low concentration. In the cases when concentration changes over time (non-steady state), the expression is called Fick's Second Law and given by;

$$\frac{\partial C_i}{\partial t} = \frac{\partial}{\partial x}\left(D_i \frac{\partial C_i}{\partial x}\right) \qquad (3)$$

Solution to this equation is sometimes found numerically since nonlinear partial differential equation with complex boundary condition cannot be solved analytically.

Primary experiments for calculating diffusion coefficients are called diffusion couple experiments. Two uniform semi-infinite discs of different composition joined at the plane x=0 is known as the diffusion couple [18]. After assembly, the couple is isothermally annealed for a specific time. By design, atoms flow unidirectionally (x direction) and interdiffuse and composition profile of each constituent develops.

Kirkendall and Smigelskas were the first researchers who reported that the diffusion rates of each constituents in a solid are different. This difference in the rate of the diffusivity of each

element is studied first by Darken (1948) [19], then Hartley and Crank (1949) [20] and defined as intrinsic diffusivity. This process of mass flow is known as the Kirkendall effect and it requires a net flux of vacancies. In many cases, including in this study, excess vacancies coalesce creating small voids, and a porous region is formed.

In a binary system, with Kirkendall effect and the Darken expression, the interdiffusion coefficient $\widetilde{D}$ can be related to the intrinsic diffusion coefficients D_A and D_B [19, 21]

$$\widetilde{D} = X_A D_B + X_B D_A \qquad (4)$$

Similarly, in binary systems, the Darken-Manning equation relates the interdiffusion coefficient $\widetilde{D}$, to mole fractions (X_A and X_B) , tracer diffusion coefficients D_A^* and D_B^*, thermodynamic factor and vacancy wind factor [22]. In Equation (5) ,$\emptyset$ is the thermodynamic factor and S is the vacancy wind effect. Generally, the vacancy wind effect is ignored assuming its contribution is small [21].

$$\widetilde{D} = (X_B . D_A^* + X_A . D_B^*) S\emptyset \qquad (5)$$

2.2.3 Impurity Diffusion Coefficient

Per Manning, when the concentration of the solute approaches to zero, both the thermodynamic factor and vacancy-wind effect becomes unity. In such cases, the interdiffusion coefficient can be taken as impurity diffusion coefficient of an infinitely dilute solute [21].

The different diffusivities and their relationships are summarized in the Table 1.

Table 1 – Summary of various diffusivities and relationships

Symbol	Name	Relationship	Reference Frame
D_A^*	Self Diffusivity	$D_i \approx \left(1 + \frac{\partial \ln \gamma_i}{\partial \ln c_i}\right)$	Crystal Frame or Laboratory Frame
D_i	Intrinsic Diffusivity	$\widetilde{D} = X_A D_B + X_B D_A$	Crystal Frame or Laboratory Frame
$\widetilde{D}$	Interdiffusivity	$\widetilde{D} = (X_B . D_A^* + X_A . D_B^*) S\emptyset$	Laboratory Frame

2.3 Kirkendall Effect

The displacement of lattice planes originating from unbalanced diffusion rate of components is commonly referred to as the Kirkendall effect [23]. Kirkendall effect can manifest itself as the development of voids [16], internal stress [24] and deformation within the material [25]. These phenomena associated with Kirkendall effects are of a concern especially in load-bearing materials used for many industrial applications, since pore formation would generally lead to "weaker" mechanical behavior, although the formation of voids has been explored to synthesize nano-scale hollow spheres [26, 27], and other complex shapes.

Kirkendall effect can be best visualized by the motion of the inert markers that positioned at the interface between the diffusion couple before the annealing process. Hartley [20] was the first to use inert TiO_2 markers. Shortly after, Smigelkas and Kirkendall [23] used inert molybdenum wire and discovered the unequal diffusivities of Cu and Zn. After the Kirkendall's experiment, it was evident that the intrinsic diffusion rates of species cannot be described by one diffusion coefficient, instead, diffusivity of each species (e.g. intrinsic diffusivity) must be determined. Since then, the inequality of diffusion rate of constituents has been widely studied using inert markers for many metallic systems, see for example [7, 8]. However, effects of marker size, amount and distribution on diffusion behavior and Kirkendall voids development have not been examined. In this experimental study, various size and distribution of Al_2O_3 makers were employed in solid-to-solid, Cu vs. Ni diffusion couple, and their effects on the development of Kirkendall voids, and determination of interdiffusion coefficients and intrinsic diffusion coefficients.

2.4 Important Fundamental Relationships

2.4.1 Onsager Phenomenological Relations

In 1931, Lars Onsager postulated that when two or more irreversible transport processes (such as heat transfer and diffusion) simultaneously take place, the processes may interfere with each other. He unified various linear laws and derived phenomenological (observation based) relations based on three major assumption[28]:

1. There is a linear relationship between the fluxes J_i and the thermodynamic forces X_i for component i in an n-component system (Equation (6).

$$J_i = \sum_{j=1}^{n} L_{ij} X_j \qquad (6)$$

In this expression, L_{ij} is called Onsager's phenomenological coefficients or transport coefficients. In a diffusion context, transport coefficients are function of temperature and pressure, but not gradient of chemical potential[29].

2. Diagonal terms in the Onsager equations, L_{ii}, connects each force with its conjugate flux. Off-diagonal terms L_{ij}, represents the influence of a force on a non-conjugate flux. For instance, electric current cause heat flow (Peltier Effect). When forces and fluxes are conjugates of each other, the transport coefficients are symmetric (also known as Onsager reciprocity theorem, Equation *(7*)). This brings a great deal of simplification to force-flux equations and enables easier calculations with experimental data.

$$L_{ij} = L_{ji} \qquad (7)$$

Thus, in a binary system, there are three transport coefficients. For a ternary system, the number of transport coefficient is six.

3. Each of the thermodynamic forces and its fluxes produce entropy (nonnegative). This is an important characteristic of irreversible processes. When thermodynamic equilibrium is achieved, entropy production vanishes[30].

All the above-mentioned flux and corresponding diffusivity must be specified relative to a particular reference frame (e.g. lattice or laboratory reference frame). For example, in a diffusion couple experiment, fluxes are measured with respect to one terminal end of the sample[31]. On the other hand, the lattice frame of reference is bound to the atomic planes. Fluxes measured with respect to laboratory frame and lattice frame are usually denoted as $\tilde{J}_A$ and J_A, respectively.

2.4.2 Boltzman-Matano Analysis

Boltzmann and Matano solved the Fick's nonlinear differential equation (also known as Fick's second law of diffusion) by first transforming it to a nonlinear ordinary differential equation utilizing scaling parameter of x (distance) over the square root of time [32], then applying initial and boundary conditions[33]. Due to its simplicity, Boltzmann-Matano method is frequently used to calculate the interdiffusion diffusion coefficient as a function of concentration. The initial contact plane of two alloys or pure materials is called Matano plane (mass balance plane) and denoted as x_o. The location of the Matano plane can be calculated by:

$$\int_{C_i^{+\infty}}^{C_i^0} x dC_i + \int_{C_i^0}^{C_i^{-\infty}} x dC_i = 0 \qquad (8)$$

Where $C_i^{+\infty}$ and $C_i^{-\infty}$ compositions of terminal ends of the diffusion couple and C_i^0 is the composition of the Matano plane. After the location of the Matano plane determined, the interdiffusion flux $\tilde{J}_i$ can be calculated using [2];

$$\tilde{J}_i = \frac{1}{2t}\int_{C_i^{\pm\infty}}^{C_i}(x - x_o)dC_i \qquad (9)$$

Finally, the interdiffusion coefficient $\widetilde{D}_i$ can be obtained by combining Fick's law with the flux equations (Equation (2) and (9));

$$\widetilde{D}_i = \frac{\frac{1}{2t}\int_{C_i^{\pm\infty}}^{C_i}(x - x_o)dC_i}{\frac{\partial C_i}{\partial x}} \qquad (10)$$

2.4.3 Belova-Sohn-Murch Formalism and Extraction of Tracer Diffusion Coefficients

Recently by Belova, Sohn and Murch developed a formalism for simultaneous measurement of isotope tracer and interdiffusion coefficients for multicomponent alloys and gave three possible experimental implementations. [6]. The formalism utilized Onsager's phenomenological relationships combined with Boltzmann-Matano transformation. One possible implementation of the formalism could employ isolated group of atoms of the same type (e.g. A1 and A2) instead of isotopes. Now, let us consider an isothermally annealed binary diffusion couple consist of alloys with compositions $A_xB_{(1-x)} - A_yB_{(1-y)}$, and within, imagine isolated group of atoms of the same type (A) which have different relative compositions and are located at two different locations of the diffusion couple. This enables these atoms to be distinguished and denoted as A1 and A2. Due to their specific location, respective thermodynamic forces (X_{A1} and X_{A2}) will not be equal. Thus, the flux of A atoms can also be split into two fluxes. Given this

information, Onsager expressions for the diffusion fluxes of the atomic component A and B in the lattice coordinate system can be written as:

$$J_{A1} = L_{A1A1}X_{A1} + L_{A1A2}X_{A2} + L_{A1B}X_B$$

$$J_{A2} = L_{A1A2}X_{A1} + L_{A2A2}X_{A2} + L_{A2B}X_B$$

$$J_B = L_{A1B}X_{A1} + L_{A2B}X_{A2} + L_{BB}X_B \qquad (11)$$

$$J_A = J_{A1} + J_{A2}$$

$$X_{A1} \neq X_{A2}$$

In an isothermal, isobaric system with a composition gradient, the driving force X_A can be expressed in terms of gradient in the chemical potential;

$$X_A = -\nabla\mu_A = -kT(\nabla\frac{c_A}{C_A} + \nabla\ln(\gamma_A)) \qquad (12)$$

where γ_A is activity coefficient of the A component, $\nabla = \partial/\partial x$, and for simplicity only unidirectional flow in x direction is considered. The two types of A atoms constitute the total A atoms, C_A.

$$C_{A1} + C_{A2} = C_A \qquad (13)$$

In a system in mechanical equilibrium, Gibbs-Duhem relation dictates that there is a restriction on the forces and it is expressed as:

$$C_{A1}X_{A1} + C_{A2}X_{A2} + C_BX_B = 0 \quad (14)$$

Since in a diffusion couple experiment, fluxes are measured in laboratory coordinate system ($\tilde{J}$), transformation between the lattice and laboratory coordinate system will be necessary. Based on the study conducted by Kirkwood et al., the fluxes with respect to any two reference frames are related [34]. Using this relationship, fluxes in the laboratory coordinates reference frame can be written as:

$$\tilde{J}_A = J_A + vc_A \quad (15)$$

$$v = (\tilde{J}_A - J_A)/c_A \quad (16)$$

$$\tilde{J}_{A1} = J_{A1} - \frac{c_{A1}}{c_A}J_A + \frac{c_{A1}}{c_A}\tilde{J}_A \quad (17)$$

where v is the lattice drift velocity, $\tilde{J}_A$ is the flux of A atoms in the laboratory coordinate system and J_A is the flux of A atoms in the lattice coordinate system. In Equation (17), there are two terms still in the lattice reference frame and need to be further replaced with experimentally measurable terms. After Darken's initial approximate proposition, Manning presented more accurate relation between the tracer diffusion coefficients and the Onsager's transport coefficients using a random alloy model, which the vacancies and different atoms were presumed to be distributed randomly [1]. By Allnatt and Lidiard, relations between the Onsager transport coefficients and tracer diffusion coefficient were derived without the dependency to the atomic model [29]. Utilizing these relationships, following equations, Equation (18), can be written:

$$L_{A1A1} = \frac{Nc_{A1}}{kT}(D_A^* + c_{A1}F_{\mathrm{A}})$$

$$L_{A2A2} = \frac{Nc_{A2}}{kT}(D_A^* + c_{A2}F_{\mathrm{A}})$$

$$L_{BB} = \frac{Nc_B}{kT}(D_B^* + c_B F_{\mathrm{B}})$$

$$L_{A1A2} = \frac{Nc_{A1}c_{A2}}{kT}F_A \qquad (18)$$

$$L_{A1B} = \frac{Nc_{A1}c_B}{kT}F_{AB}$$

$$L_{A2B} = \frac{Nc_{A2}c_B}{kT}F_{AB}$$

where N is the number of lattice sites, D_A^* and D_B^* are the tracer diffusion coefficients, F_{A} is correlation function between the movement of A atoms, F_{B} is correlation function between the movements of B atoms and F_{AB} is cross correlation function between the movements of A and B atoms. After the transport coefficient terms that are in the Onsager's flux equations and flux equation in the laboratory reference frame are combined, following flux equation can be obtained, Equation (19);

$$\tilde{J}_{A1} = \frac{N}{kT}D_A^* c_{A1}(X_{A1} - X_A) + \frac{c_{A1}}{c_A}\tilde{J}_A; \qquad (19)$$

$$X_A = -\nabla\mu_A = -kT(\nabla\frac{C_A}{C_A} + \nabla\ln(\gamma_A)) \qquad (20)$$

Again, further replacement of Equation (20) thermodynamic forces (X) in the flux equation;

$$\tilde{J}_{A1} = -ND_A^*\left(\nabla c_{A1} - \frac{c_{A1}}{c_A}\nabla c_A\right) + \frac{c_{A1}}{c_A}\tilde{J}_A$$
$$\tilde{J}_{A2} = -ND_A^*\left(\nabla c_{A2} - \frac{c_{A2}}{c_A}\nabla c_A\right) + \frac{c_{A2}}{c_A}\tilde{J}_A; \quad (21)$$

In Equation (21) all the terms are measurable in the laboratory reference frame once the concentration profiles are extracted from the diffusion experiments.

Now, assuming the diffusion couple was annealed for time t, the diffusion equations (Fick's second law) for A (Equation (22)), A1 (Equation (23)) and B (Equation (24)) can then be written as:

$$\frac{\partial c_A}{\partial t} = -\nabla J_A^0/N; \quad (22)$$

$$\frac{\partial c_{A1}}{\partial t} = \nabla\left[D_A^*\nabla c_{A1} + \left(D_A^* - \widetilde{D}\right)\frac{c_{A1}}{c_A}\nabla c_B\right] \quad (23)$$

$$\frac{\partial c_B}{\partial t} = \nabla(\widetilde{D}\nabla c_B) \quad (24)$$

When Boltzmann transformation Equation (25) is applied to Equation (23),

$$\lambda = \frac{x}{\sqrt{t}} \quad (25)$$

$$c_{A1} = \frac{f(\lambda)}{\sqrt{t}} \tag{26}$$

$$\frac{\partial}{\partial x} = \frac{1}{\sqrt{t}}\frac{d}{d\lambda}$$
$$\frac{\partial}{\partial t} = \frac{\lambda}{2t}\frac{d}{d\lambda} \tag{27}$$

where f, $\widetilde{D}$ and D_A^* all function of λ due to their relationships.

$$-\left(f + \lambda\frac{df}{d\lambda}\right) = 2\frac{d}{d\lambda}\left\{D_A^*\frac{df}{d\lambda} + \left(D_A^* - \widetilde{D}\right)\frac{f}{c_A}\frac{dc_B}{d\lambda}\right\} \tag{28}$$

$$-\frac{d(\lambda f)}{d\lambda} = 2\frac{d}{d\lambda}\left\{D_A^*\frac{df}{d\lambda} + \left(D_A^* - \widetilde{D}\right)\frac{f}{c_A}\frac{dc_B}{d\lambda}\right\} \tag{29}$$

After integration of Equation (29) with the variable λ,

$$-\frac{\lambda f}{2} = D_A^*\frac{df}{d\lambda} + \left(D_A^* - \widetilde{D}\right)\frac{f}{c_A}\frac{dc_B}{d\lambda} \tag{30}$$

$$\frac{dc_B}{d\lambda} = -\frac{dc_A}{d\lambda} \tag{31}$$

After dividing Equation (30) by f, and using Equation (32);

$$-\frac{\lambda}{2} = D_A^* \frac{dln(c_{A1})}{d\lambda} - \left(D_A^* - \widetilde{D}\right)\frac{dln(c_A)}{d\lambda} \qquad (32)$$

Since anneal time will be constant, Equation (32) will get the form of Equation (33);

$$-\frac{x}{2t} = D_A^* \frac{dln(c_{A1})}{dx} - \left(D_A^* - \widetilde{D}\right)\frac{dln(c_A)}{dx} \qquad (33)$$

After isolating the tracer diffusion coefficient on the left and re-arranging the terms, Equation (34) and (35) can be obtained.

$$D_A^* = -\left(\frac{x}{2t} + \widetilde{D}\ \frac{d\ \ln(c_A)}{dx}\right)\Big/\left(\frac{d\ ln(c_{A1})}{dx} - \frac{d\ ln(c_A)}{dx}\right) \qquad (34)$$

$$D_A^* = -\left(\frac{xc_{A1}}{2t} + \widetilde{D}\ \frac{c_{A1}}{c_A}\frac{dc_A}{dx}\right)\Big/\left(\frac{d\ c_{A1}}{dx} - \frac{c_{A1}}{c_A}\frac{d\ c_A}{dx}\right) \qquad (35)$$

The location of the Matano plane must be determined in the Boltzmann –Matano analysis. As in the Boltzmann-Matano analysis, similarly, here, origin of the λ axis must be determined. Since Equation (30) does not include any intergral terms, origin of the λ can be taken as λ+a*. Here, a* is a constant number represents the shift of the position of the λ. When λ term in Equation (32) is replaced by λ+a* term, Equation (36) is obtained.

$$-\frac{\lambda + a^*}{2} = D_A^* \frac{dln(c_{A1})}{d\lambda} - \left(D_A^* - \widetilde{D}\right)\frac{dln(c_A)}{d\lambda} \qquad (36)$$

For organization of the equation (36), a = a*√t relationship can be written where a is also a constant. This constant in the equation plays a role solely to control the sign of the numerator and denominator. Thus, when determining the value of "a" should be taken in a way that resulting tracer coefficient will always be positive. Finally, the equation can be written as below Equation (37).

$$D_A^* = -\left(\frac{(x+a)}{2t} + \widetilde{D}\ \frac{dlnc_{A2}}{dx}\right)\Big/\left(\frac{d\ln(c_{A1}/c_{A2})}{dx}\right) \qquad (37)$$

CHAPTER 3 EXPERIMENTAL METHODS

3.1 Determination of geometry and compositions for the experiments

For this set of experiments three Cu-Ni alloys with varying compositions (Cu25Ni, Cu50Ni, Cu75Ni), pure Cu and pure Ni discs are used for diffusion couple preparations. Cu-Ni alloys are selected because large number of accurate diffusion data is present in the literature. In order to successfully apply the formalism, the alloys in the diffusion couple have to be arranged with a stacking sequence for the purpose of simultaneous measurement interdiffusion and isotopic diffusion profile. Figure 3 shows a typical arrangement of diffusion couple assembly and corresponding concentration profiles before and after heat treatment. A thin film of isotopic Cu was placed between 'Metal 2' and 'Metal 3', while 'Metal 1' and 'Metal 2' were in contact with one another without the isotopic thin film. Thus, only interdiffusion takes place between 'Metal 1' and 'Metal 2', while the thin-film Cu isotopic diffusion occurs in addition to the interdiffusion between 'Metal 2' and 'Metal 3'. Figure 3 schematically illustrates this arrangement.

In order to obtain the compositional dependence of the tracer diffusion coefficient, alloy stacking geometries varied for each experiment. A list of all diffusion couples assembled, annealed and analyzed in this study is given in Table 2. To further verify the repeatability and consistency of this study, diffusion couple experiments, 2, 4, 7 and 9 were repeated, so that the standard deviation of the tracer diffusion coefficient can also be found. These repeated couples were denoted, for example, 2A and 2B for diffusion couple experiment number two (2*).

Table 2 – Stacking sequence, anneal temperatures and anneal times of diffusion couples assembled with Cu thin film

Couple	Stacking Sequence				Temp (°C)	Time (s)
	Metal 1	Metal 2	Thin Film	Metal 3		
1	Cu50Ni	Cu25Ni	Cu	Cu50Ni	1000	900
2*	Cu50Ni	Cu25Ni	Cu	Cu50Ni	900	900
3	Cu50Ni	Cu25Ni	Cu	Cu50Ni	800	5400
4*	Cu75Ni	Cu50Ni	Cu	Cu75Ni	1000	7200
5	Cu75Ni	Cu50Ni	Cu	Cu75Ni	900	18000
6	Cu75Ni	Cu50Ni	Cu	Cu75Ni	800	75600
7*	Cu75Ni	Ni	Cu	Cu75Ni	1000	3600
8	Cu75Ni	Ni	Cu	Cu75Ni	900	3600
9*	Cu75Ni	Ni	Cu	Cu75Ni	800	10800

In the binary Cu-Ni system, Cu is the faster diffusion species. There is almost an order of magnitude difference in the intrinsic diffusivities of Cu and Ni [35]. To further verify the repeatability and consistency of this study, diffusion couples containing Ni thin film were also assembled. The stacking sequence, anneal time and the temperature of the diffusion couples assembled with Ni thin film were given in the Table 3.

Table 3 - Stacking sequence, anneal temperatures and anneal times of diffusion couples assembled with Ni thin film

Couple	Stacking Sequences				Temp (°C)	Time (sec)
	Metal 1	**Metal 2**	**Thin Film**	**Metal 3**		
10	Cu25Ni	Cu50Ni	Ni	Cu25Ni	1000	300
11	Cu25Ni	Cu50Ni	Ni	Cu25Ni	900	5400
12	Cu25Ni	Cu50Ni	Ni	Cu25Ni	800	21600
13	Cu50Ni	Cu75Ni	Ni	Cu50Ni	1000	1800
14	Cu50Ni	Cu75Ni	Ni	Cu50Ni	900	1800
15	Cu50Ni	Cu75Ni	Ni	Cu50Ni	800	158400
16	Cu	Cu25Ni	Ni	Cu	1000	600
17	Cu	Cu25Ni	Ni	Cu	900	600
18	Cu	Cu25Ni	Ni	Cu	800	3600

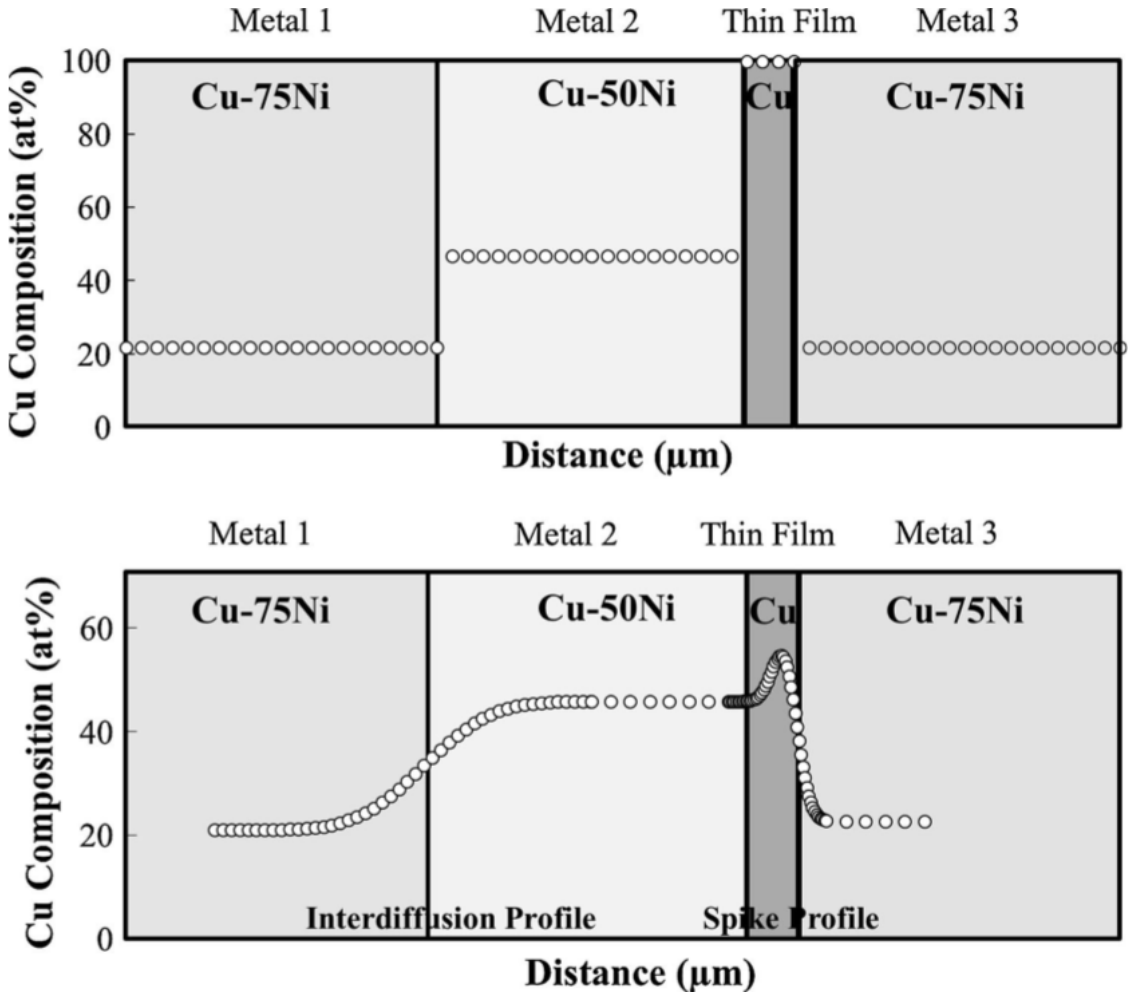

Figure 3 – Schematic representation of diffusion couple and corresponding concentration profile before and after isothermal annealing

3.2 Calculation of concentration profiles

In order to determine the optimum temperature and the anneal time, spreadsheets were prepared in a way that, corresponding concentration profiles can be plotted when the temperature, anneal time and film thickness were entered.

3.3 Preparation of Samples for Diffusion Studies

Each alloy surfaces were metallographically ground with 240, 600, 800 and 1200 grit SiC papers to achieve a flat and smooth surface for the diffusion couple assembly. During grinding process, high purity ethanol was used as lubricant. Final polish was performed on a microcloth dispersed with 1µm diamond paste lubricated with mineral oil. Samples were then ultrasonically cleaned with high purity ethanol. Within prepared samples, 13 of them were selected to be deposited with pure Cu, including additional diffusion couples. Same sample preparation procedure was followed for the samples prepared for Ni tracer calculations, Thirteen of the prepared couples were selected to be deposited with pure Ni thin film,.

3.4 Utilization of E-beam PVD technique for Cu thin film deposition

E-beam PVD technique is employed for Cu and Ni deposition. Deposition rate monitored by using an oscillating crystal. The thickness of the deposited film was determined by the resonant frequency of the crystal shifts proportional to the thickness of the deposited film. Target thickness was 3 µm for Cu thin film and 2 µm for Ni thin film. Based on the target thickness, the Cu and Ni deposition times were 80 minutes and 120 minutes respectively. Cu deposition

parameters were as follows; main chamber pressure: $1.2x10^{-7}$ Torr, power: 10kV, current: 320 mA, deposition rate: 1 to 1.4 Aº/sec. For Ni deposition, deposition rate was 0.7 Aº /sec.

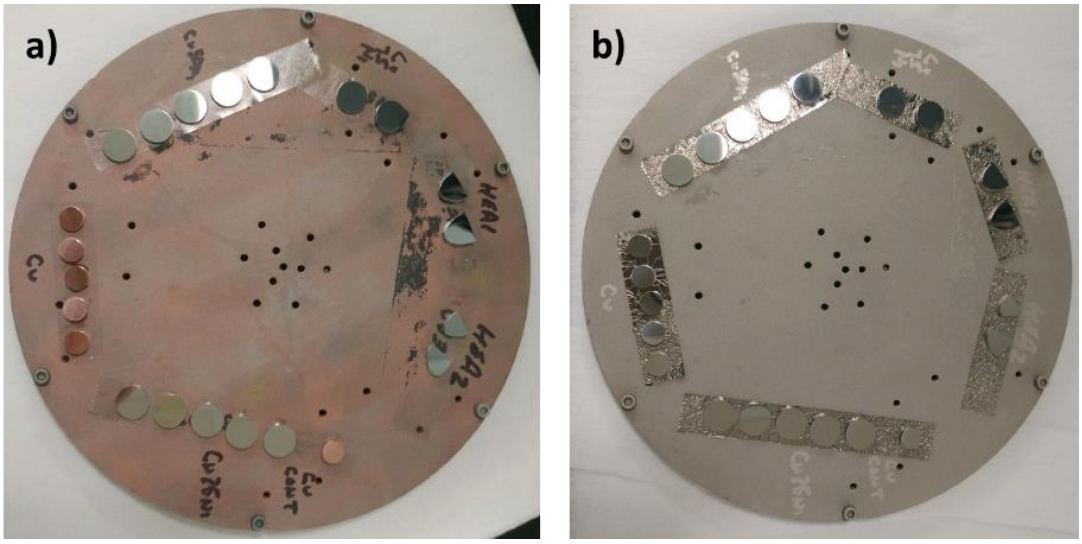

Figure 4 – Polished samples a) before and b) after Ni E-Beam PVD deposition

3.5 Thin film thickness measurement via Focused Ion Beam (FIB)

The actual thickness of the film was measured on a control sample via FIB. In order to protect the surface from the ion damage, first, 12 µm long, 2 µm wide and 1.5 µm thick Pt was deposited on the surface of the samples. 12 µm x 7 µm x 5 µm trench was patterned in front of the Pt deposition. After the trench was formed, FIB micrographs were taken at 45° and total thickness of the film was calculated based on the geometry (Figure 5). Deposited film thickness was measured as 3.2 µm. According to actual film thicknesses, anneal times were calculated.

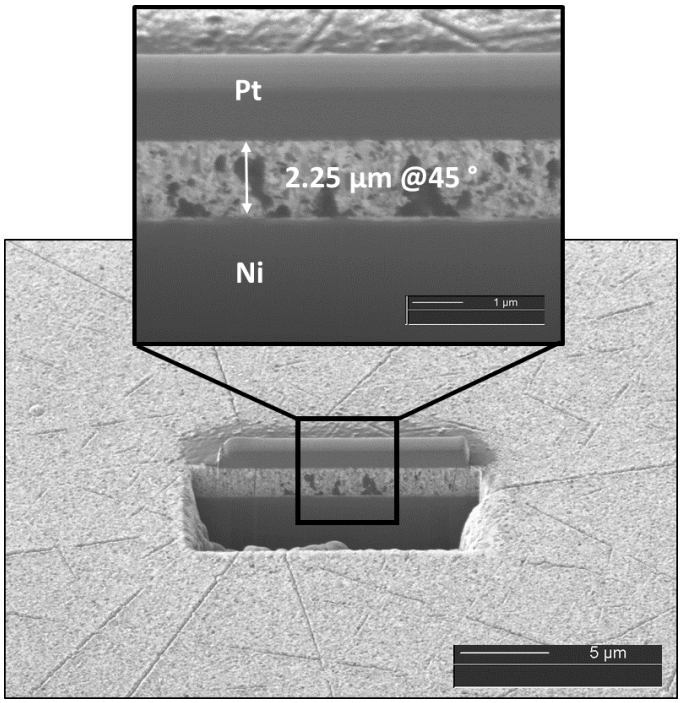

Figure 5- FIB micrograph taken at a 45° angle for calculation of thickness of the deposited thin film

3.6 Marker (Al_2O_3) Selection and Placement

After Cu and Ni rods were sectioned into 3-mm thick discs. The disc surfaces were metallographically polished down to 1200 grit using SiC polishing paper, and further polished using a micro cloth and 1 µm diamond paste. The Al_2O_3 inert markers varying in size, 1, 3, 5 and 9 µm were suspended in 15 ml absolute ethanol solution (200 proof) with the amount ranging from 0.01 to 0.5 grams, which corresponds to concentration ranging from 0.67 mg/ml to 33.33 mg/ml. The Al_2O_3 particles employed in this study are α-Al_2O_3 typically used in metallographic preparation (e.g., 1 µm and 3 µm particles from Leco Inc., and 5 µm and 9 µm particles from

Allied Inc.). Suspension was placed in an ultrasonic cleaner for 5 minutes to ensure the all of the Al_2O_3 particles were de-agglomerated. Polished metal (Ni) was then immersed in the suspension, removed and quickly dried under a lamp, leaving only Al_2O_3 particles on the surface. Variations in the amount and distribution of Al_2O_3 markers on the Ni surface were documented by optical microscopy before the assembly of solid-to-solid diffusion couple. Figure 6 illustrates the procedure diffusion couple assembly with varying amounts of markers, and diffusion couple experiments carried out as functions of marker size and marker amount (i.e., concentration in ethanol) are reported in Table 4.

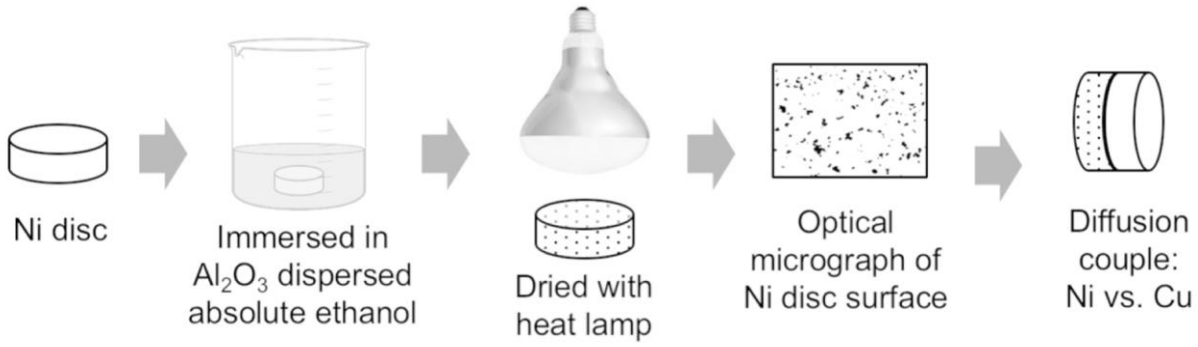

Figure 6 - A schematic diagram illustrating the procedure for diffusion couple assembly with varying amounts of Al_2O_3 markers.

Table 4 - Experimental Cu vs. Ni diffusion couple matrix detailing size, amount and concentration of Al_2O_3 marker particles.

Couple	Marker Size (µm)	Marker Amount (mg)	Marker Concentration (mg/ml)
1	No marker	-	0
2	1	10	0.67
3		25	1.67
4		50	3.33
5		60	4.00
6		75	5.00
7		100	6.67
8		500	33.33
9	3	10	0.67
10		75	5.00
11*		500	33.33
12	5	10	0.67
13		25	1.67
14		50	3.33
15		60	4.00
16		75	5.00
17		100	6.67
18		500	33.33
19	9	10	0.67
20		75	5.00
21		500	33.33

*Two diffusion couples were assembled and annealed: one was water quenched and one was furnace cooled.

3.7 Diffusion Couple Assembly and Annealing

Polished alloy surfaces were attached then contained in stainless steel jig with alumina (Al_2O_3) spacers to avoid any reaction between the stainless steel and the diffusion couple (Figure 7). The assembled diffusion couples were encapsulated in quartz capsules using oxy-propylene torch. Prior to sealing, the capsule was repeatedly evacuated and flushed with argon and H_2. Samples were sealed when high vacuum value of at least $8x10^{-6}$ torr was achieved as shown in the Figure 8

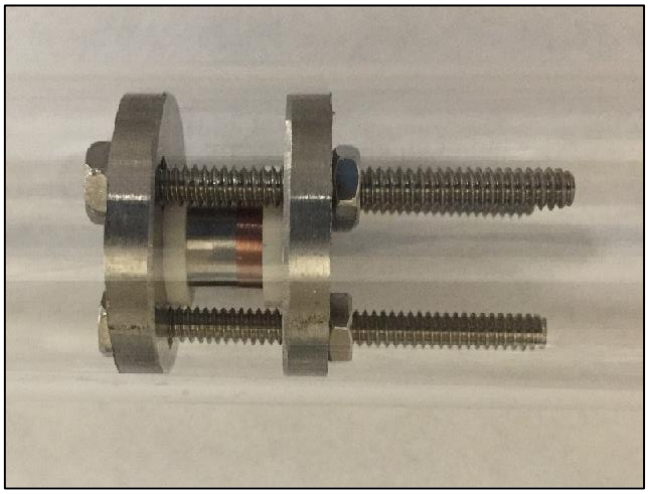

Figure 7 -Diffusion couple contained in a stainless-steel jig and alumina spacers

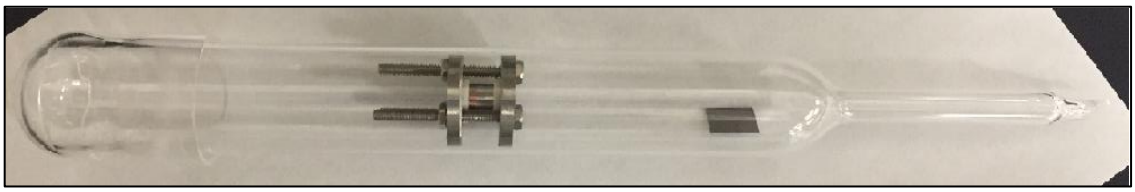

Figure 8 - Quartz capsule for encapsulation of diffusion couple under vacuum or inert atmosphere to prevent oxidation during high temperature anneal.

The annealing of the diffusion couples was performed with Lindberg/Blue™ three-zone tube furnace. The couples were isothermally annealed at proposed temperature. Table 2 shows the annealing temperature and time for each diffusion couple.

After annealing, the quartz capsules were carefully removed from the furnace and quenched in cold water by breaking the capsules in the water. After quenching, the diffusion couples were mounted in epoxy, cross-sectioned with a diamond blade and metallographically polished to 1 μm for characterization.

3.8 Characterization of Diffusion Couples

The interdiffusion zone was examined by Zeiss Ultra-55 field emission scanning electron microscopy (FE-SEM) equipped with X-ray energy dispersive spectroscopy (XEDS). Standard-less quantification XEDS is employed to obtain a concentration profiles across the both diffusion zones: one with interdiffusion only and the other with imposed thin film (e.g., tracer and interdiffusion). Concentration profiles extracted from EDS data were fitted using OriginPro 8.5 software. Equation (38) is used as non-linear curve fitting of the concentration profiles [37]. Backscatter electron micrograph and superimposed concentration profile of the diffusion couple (Cu75Ni-Cu50Ni-Cu-Cu75Ni) annealed at 1000°C for 7200 seconds is shown in the Figure 9.

$$c(x) = \frac{p_1 + p_3 x + p_5 x^2 + p_7 x^3}{1 + p_2 x + p_4 x^2 + p_6 x^3} \qquad (38)$$

When performing nonlinear curve fitting, an iterative procedure is employed to obtain the optimal parameter values. Goodness of the fit was determined by reduced chi-square and adjusted R-square values (approximately unity).

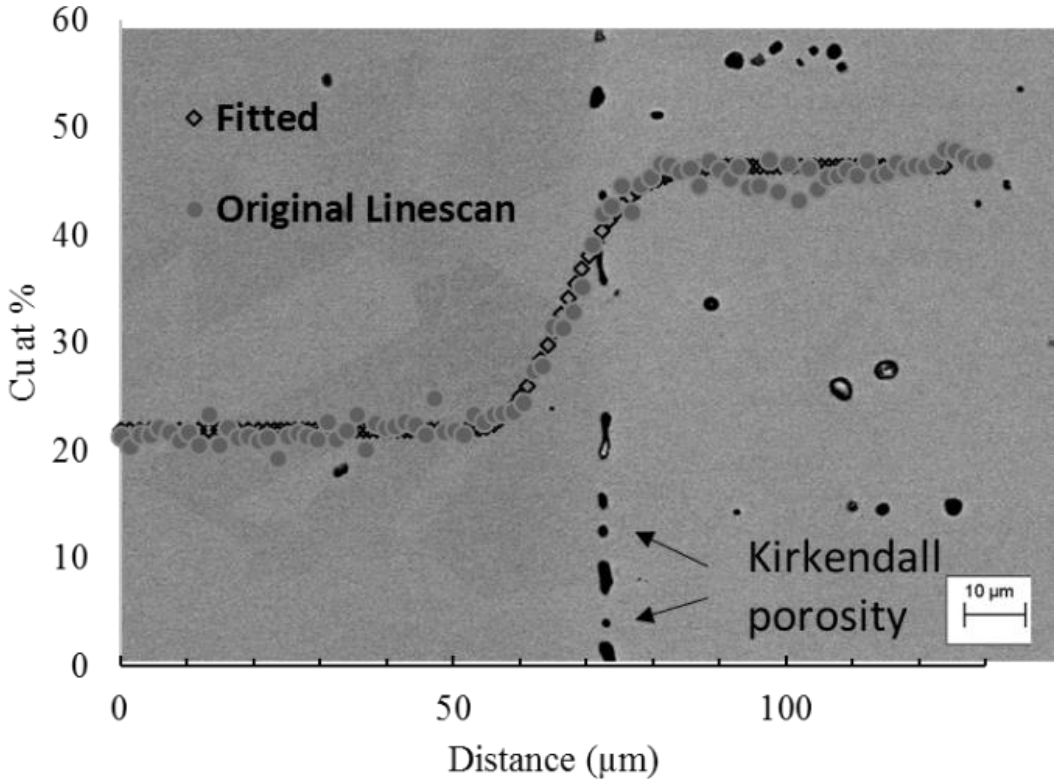

Figure 9 – Backscatter electron micrograph and superimposed concentration profile of the diffusion couple(Cu75Ni-Cu50Ni-Cu-Cu75Ni) annealed at 1000°C for 7200 s

3.9 Shape of Kirkendall Voids

A shape factor, f_1 [36], was employed to document the development of Kirkendall voids. In this analysis, an individual Kirkendall pore is converted into a binary form or image. Shape factor, f_1, typically described as elongation is defined as:

$$f_1 = \frac{a}{b} \tag{39}$$

where a and b are the length and width of the minimum bounding rectangle. Shape factor, f_1 takes the value of 1 for an ideal circle or a square, and greater values for elongated shapes.

CHAPTER 4 EXPERIMENTAL RESULTS

4.1 Marker Distribution

Aforementioned, prior to diffusion couple assembly, variation in the amount and distribution of Al_2O_3 markers on the Ni surface were documented by optical microscopy before the assembly of solid-to-solid diffusion couple. Areal coverage of Al_2O_3 marker particles on the Ni surface analyzed from optical micrographs is reported in Table 5 for all diffusion couples.

Figure 10 presents selected optical micrographs from Ni surface that show the distribution of 1-μm Al_2O_3 marker particles as well as the corresponding Ni surface coverage by the Al_2O_3 marker particles. An increase in concentration of 1-μm Al_2O_3 marker particles from 3.33 mg/ml to 6.67 mg/ml clearly increased the marker coverage on the Ni surface from 6 up to 35 percent as presented in Figure 10(d). A significant and non-uniform agglomeration of Al_2O_3 marker particles on the Ni surface was also observed starting with 6.67 mg/ml as shown in Figure 10(c).

Table 5 - Surface area coverage analyzed with optical micrographs of Cu vs. Ni diffusion couples

Couple	Marker Size (μm)	Marker Amount (mg)	Marker Concentration (mg/ml)	Areal Coverage on Ni Surface (percent)
1	No marker	-	0	0
2	1	10	0.67	6.11
3		25	1.67	7.27
4		50	3.33	9.96
5		60	4.00	18.54
6		75	5.00	22.84
7		100	6.67	28.7
8		500	33.33	34.8
9	3	10	0.67	4.04
10		75	5.00	23.40
11*		500	33.33	67.08
12	5	10	0.67	7.28
13		25	1.67	13.96
14		50	3.33	20.61
15		60	4.00	28.27
16		75	5.00	41.40
17		100	6.67	51.35
18		500	33.33	81.65
19	9	10	0.67	11.11
20		75	5.00	18.26
21		500	33.33	89.11

*Two diffusion couples were assembled and annealed: one was water quenched and one was furnace cooled.

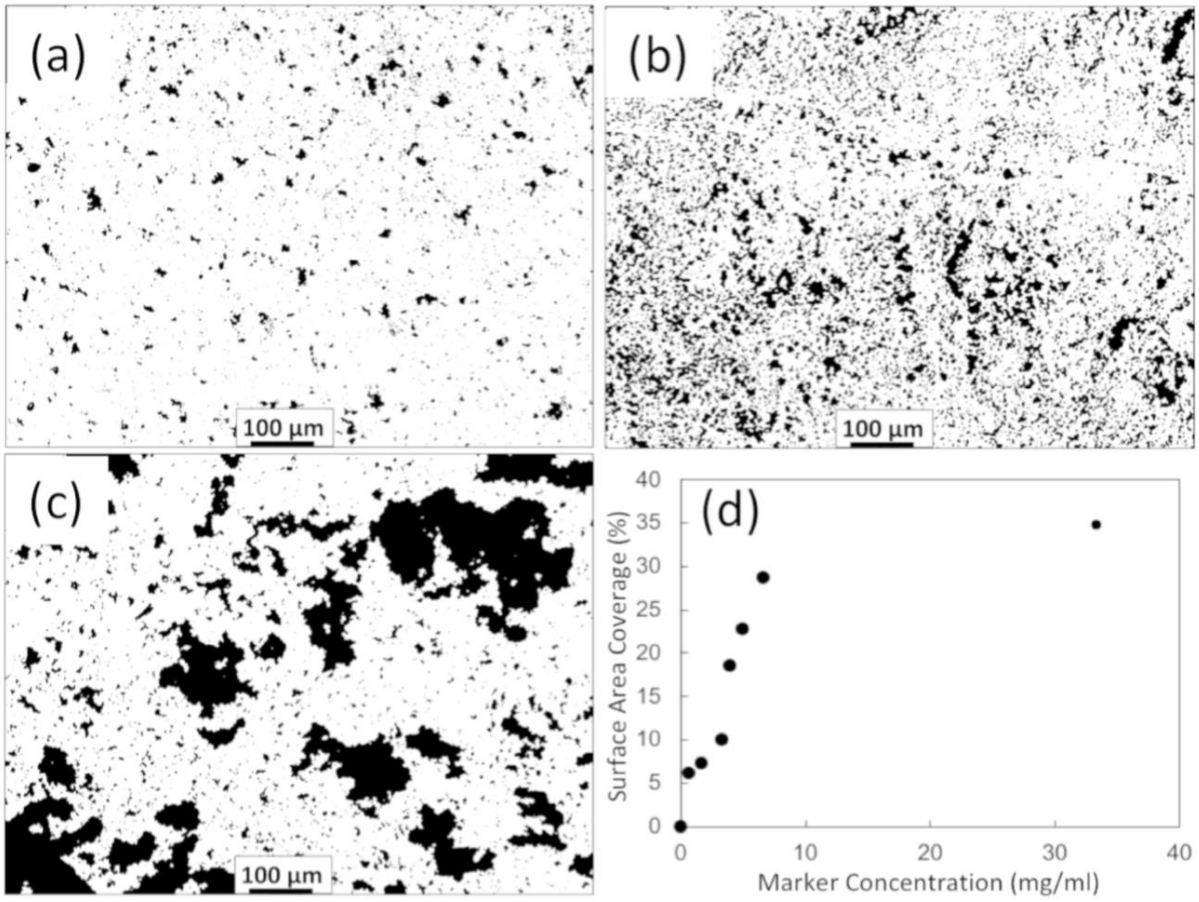

Figure 10 - Optical micrographs of 1-µm Al_2O_3 marker distributed on the Ni surface from marker concentration of (a) 3.33 mg/ml, (b) 5.00 mg/ml, and (c) 6.67 mg/ml, and (d) the corresponding Ni surface area coverage by the 1µm Al_2O_3 marker particles.

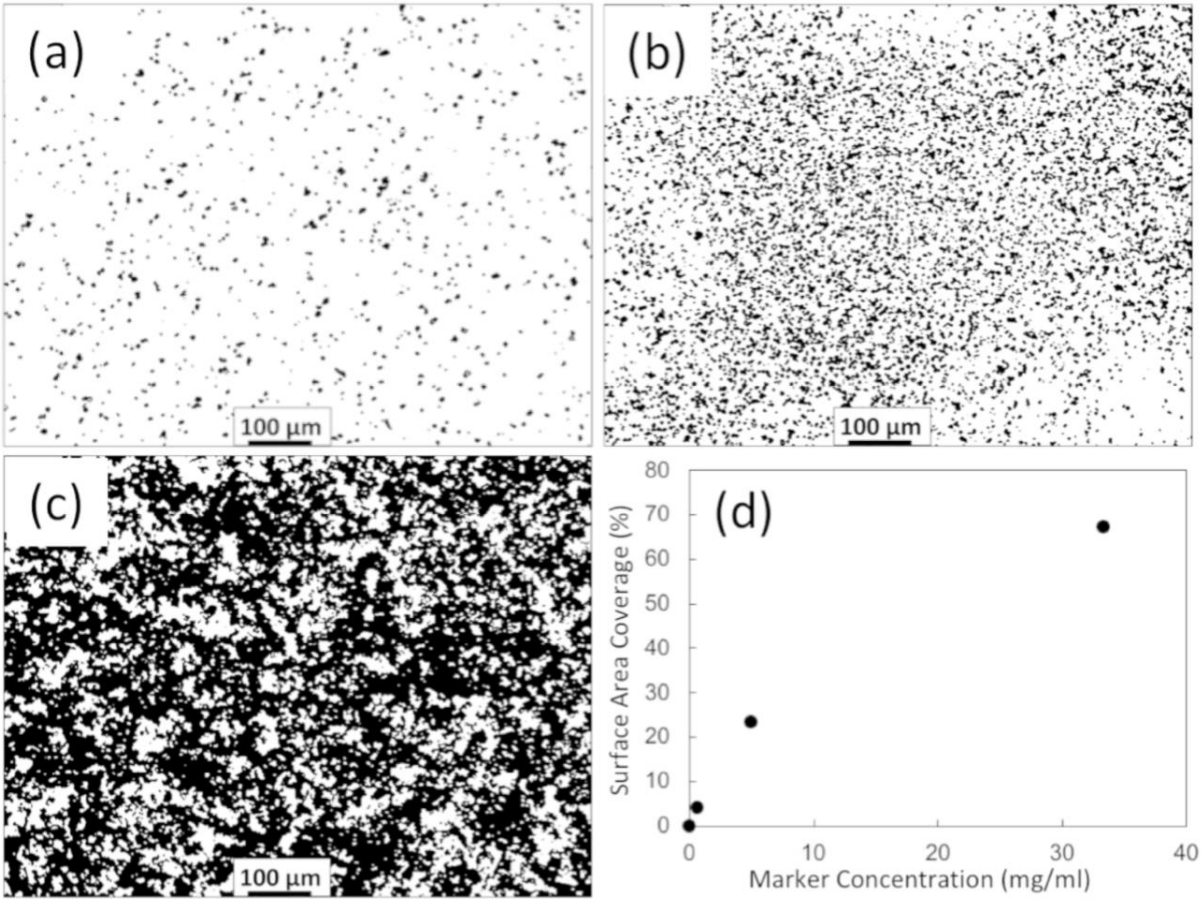

Figure 11 - Optical micrographs of 3-µm Al_2O_3 marker distributed on the Ni surface from marker concentration of (a) 0.67 mg/ml, (b) 5.00 mg/ml, and (c) 33.33 mg/ml, and (d) the corresponding Ni surface area coverage by the 3-µm Al_2O_3 marker particles.

Figure 11 presents optical micrographs of Ni surface that shows the distribution of 3-µm Al_2O_3 marker particles. A significant areal coverage up to 70 percent was observed with a concentration of 33.33 mg/ml. As the size of the Al_2O_3 marker particle increased to 5 µm and 9 µm, a further increase in areal coverage was observed as presented in Figure 12 and Figure 13,

respectively. Agglomeration of Al_2O_3 marker particles was observed to be more uniform with larger particle size. Regardless of size, areal coverage was, in general, parabolically related to the amount of Al_2O_3 marker particles placed in 15 ml ethanol, i.e., marker concentration reported in Table 5, as presented in Figures Figure 10(d), Figure 11(d), Figure 12(d) and Figure 13(d).

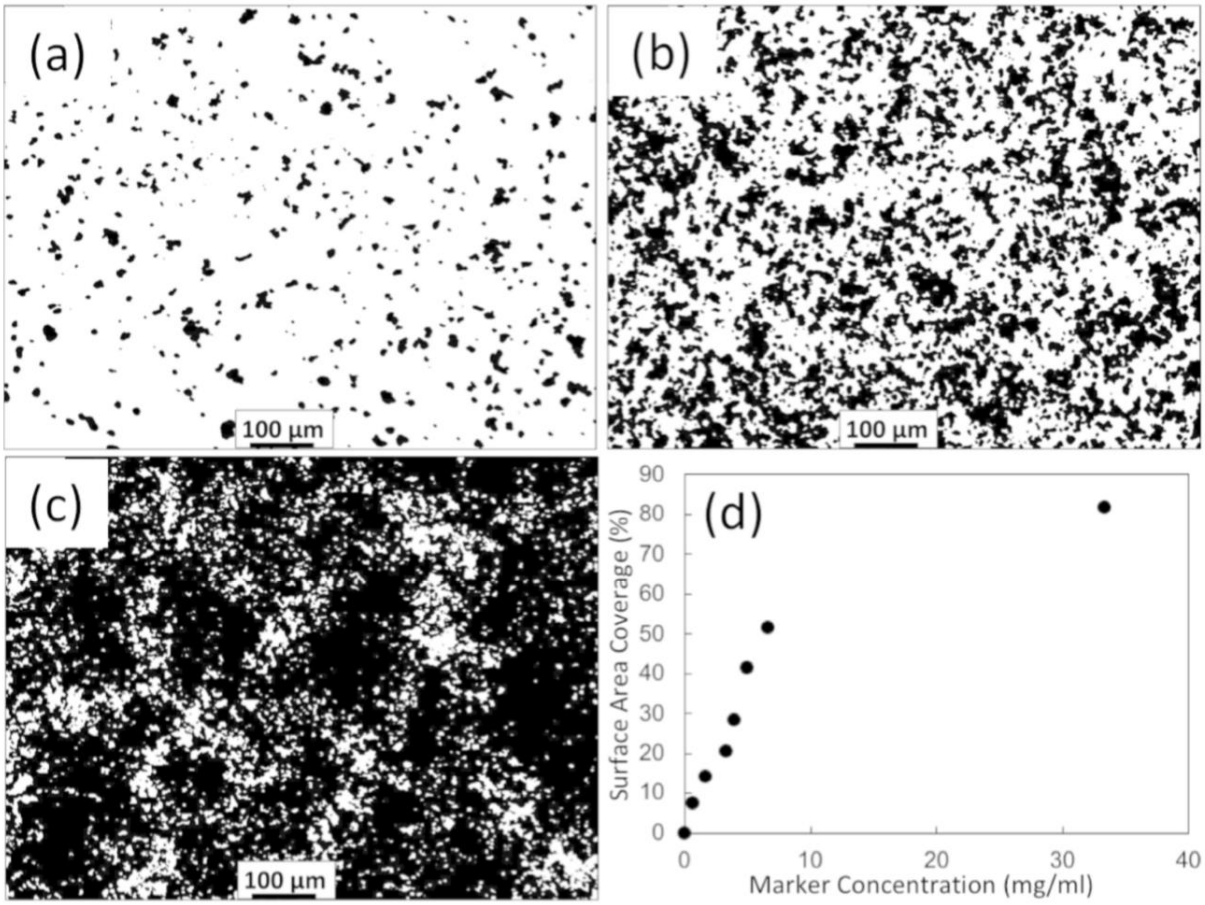

Figure 12 - Optical micrographs of 5-µm Al_2O_3 marker distributed on the Ni surface from marker concentration of (a) 0.67 mg/ml, (b) 5.00 mg/ml, and (c) 33.33 mg/ml, and (d) the corresponding Ni surface area coverage by the 5-µm Al_2O_3 marker particles.

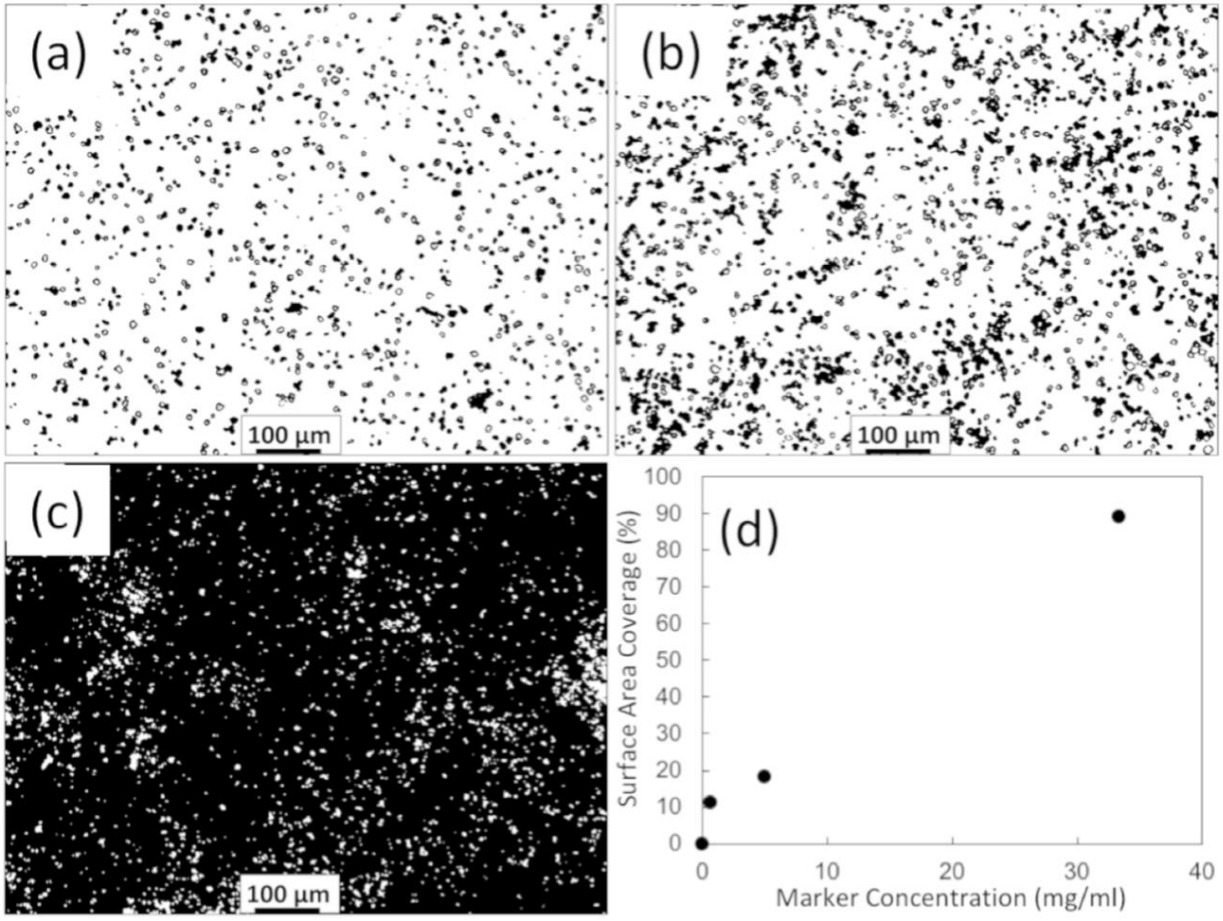

Figure 13 - Optical micrographs of 9-µm Al_2O_3 marker distributed on the Ni surface from marker concentration of (a) 0.67 mg/ml, (b) 5.00 mg/ml, and (c) 33.33 mg/ml, and (d) the corresponding Ni surface area coverage by the 9-µm Al_2O_3 marker particles.

4.2 Kirkendall Voids

Figure 14 presents backscatter electron micrograph from the interdiffusion zone of Cu vs. Ni, solid-to-solid diffusion couple that was assembled without any markers, and annealed at 1000°C for 48 hours. In the Cu-Ni system, it has been previously documented that Cu intrinsically diffuses faster than Ni, and Kirkendall voids forms on the Cu-rich side due to the coalescence of excess vacancies. At least from the cross-section presented in Figure 14, these voids appeared to be circular, and not interconnected, but exist over a range of distance approximately up to 50 μm.

Figure 15 presents backscatter electron micrographs from the interdiffusion zone of Cu vs. Ni, solid-to-solid diffusion couples that were assembled with 1 μm Al_2O_3 marker particles, and annealed at 1000°C for 48 hours. Kirkendall voids were circular and separated with marker concentration from 0.67 to 1.67 mg/ml, but interconnection of voids that lead to elongated voids appeared with marker concentration of 3.33 mg/ml as presented in Figure 15(c) and Figure 15(d). As the marker amount (or cross-sectional area coverage) increased, the Kirkendall voids became more elongated and interconnected. Figure 15(h) shows that Kirkendall void developed into a gap between Ni and Cu.

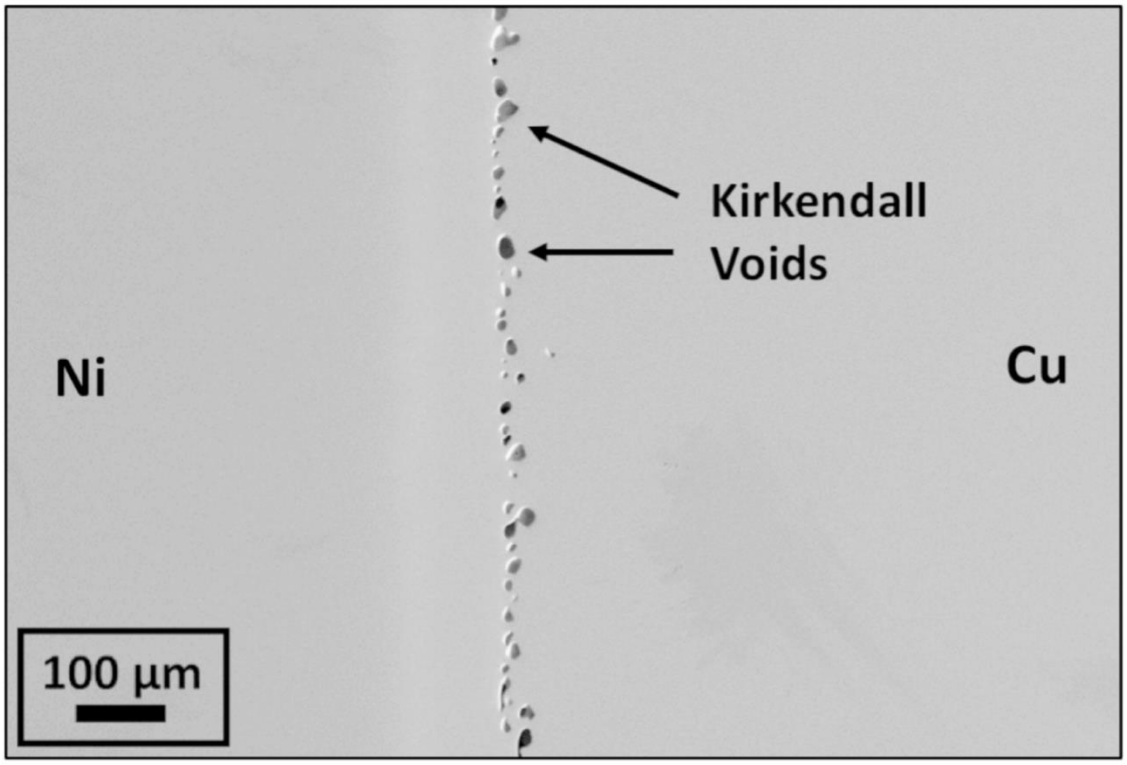

Figure 14 - Backscatter electron micrographs of Kirkendall voids development in the Cu vs. Ni diffusion couple assembled with no markers and annealed at 1000°C for 48 hours.

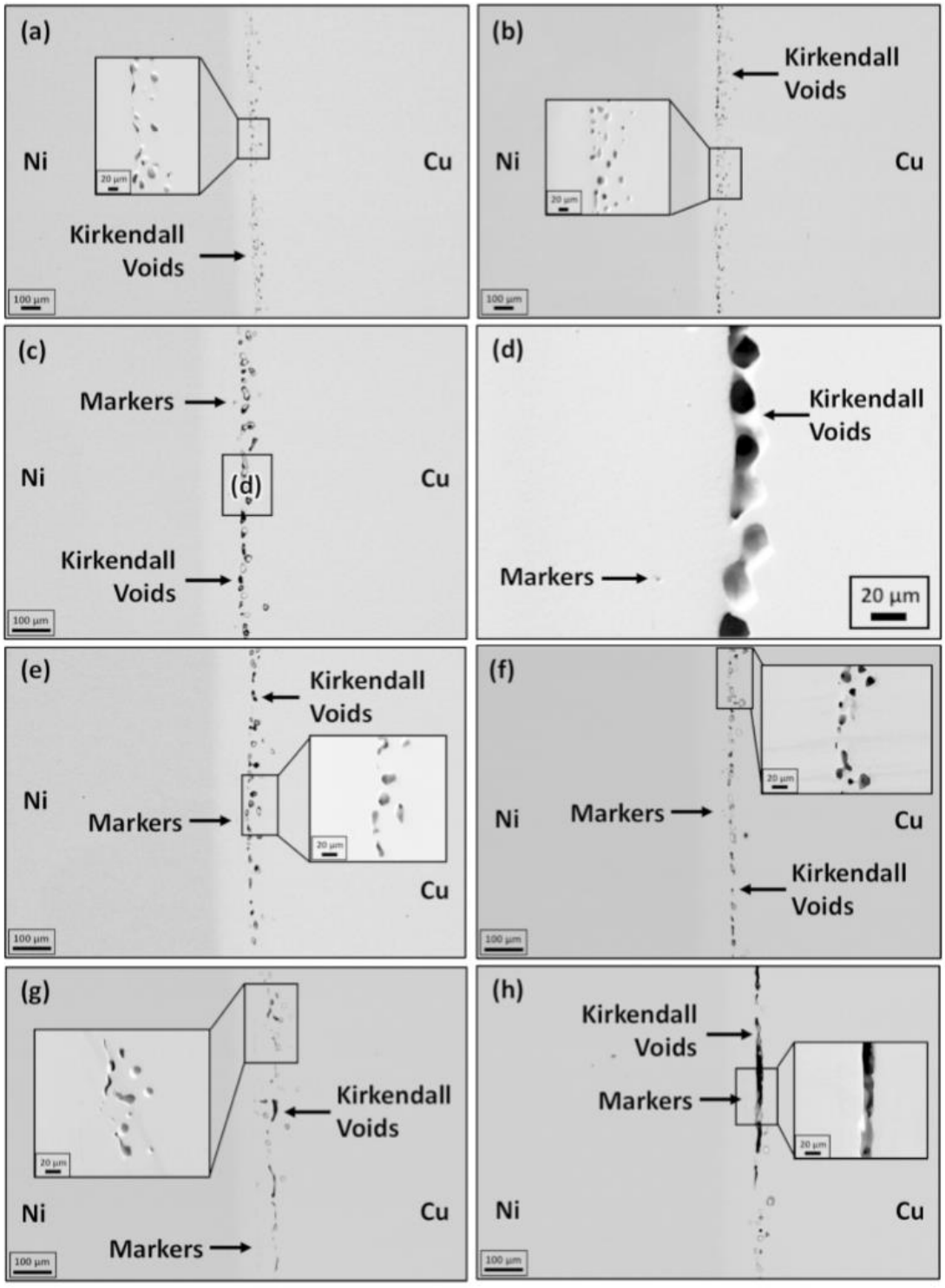
(a)
Ni
Cu
Kirkendall
Voids
100 µm
20 µm
(b)
Kirkendall
Voids
Ni
Cu
100 µm
20 µm
(c)
Markers
Ni
(d)
Cu
Kirkendall
Voids
100 µm
(d)
Kirkendall
Voids
Markers
20 µm
(e)
Kirkendall
Voids
Ni
Markers
Cu
100 µm
20 µm
(f)
Ni
Markers
Cu
Kirkendall
Voids
100 µm
20 µm
(g)
Kirkendall
Voids
Ni
Cu
Markers
100 µm
20 µm
(h)
Kirkendall
Voids
Markers
Ni
Cu
100 µm
20 µm

Figure 15 - Backscatter electron micrographs of Kirkendall voids development in the Cu vs. Ni diffusion couples annealed at 1000°C for 48 hours. Diffusion couples were assembled with 1 µm marker concentration (mg/ml) of (a) 0.67, (b) 1.67 (c,d) 3.33, (e) 4.00, (f) 5.00, (g) 6.67 and (h) 33.33.

Figure 16 presents backscatter electron micrographs from the interdiffusion zone of Cu vs. Ni, solid-to-solid diffusion couples that were assembled with 3-µm Al_2O_3 marker particles and annealed at 1000°C for 48 hours. At lower concentrations, both markers and Kirkendall voids, both circular and elongated, were observed as shown in Figure 16(a) and Figure 16(b). However, with the highest concentration of marker at 33.33 mg/ml, i.e., over 67 percent areal coverage on Ni as shown in Figure 11(d), markers appeared as a metal+Al_2O_3 layer with an observable thickness, and Kirkendall voids appeared as a linear feature normal to the diffusional flux as shown in Figure 16(c).

Similar observation was made from the Cu vs. Ni couples with 5-µm and 9-µm Al_2O_3 marker particles. Circular and elongated Kirkendall voids were observed at lower concentration of Al_2O_3 marker particles, but as the amount of Al_2O_3 marker particles increased, i.e., more areal coverage on Ni as shown in Figure 12 and Figure 13, markers appeared as a metal+Al_2O_3 layer with an observable thickness, and Kirkendall voids appeared as a linear feature, e.g., some not discernable as voids, normal to the diffusional flux as shown in Figure 17(f), Figure 17(g), Figure 17(h) and Figure 18(d).

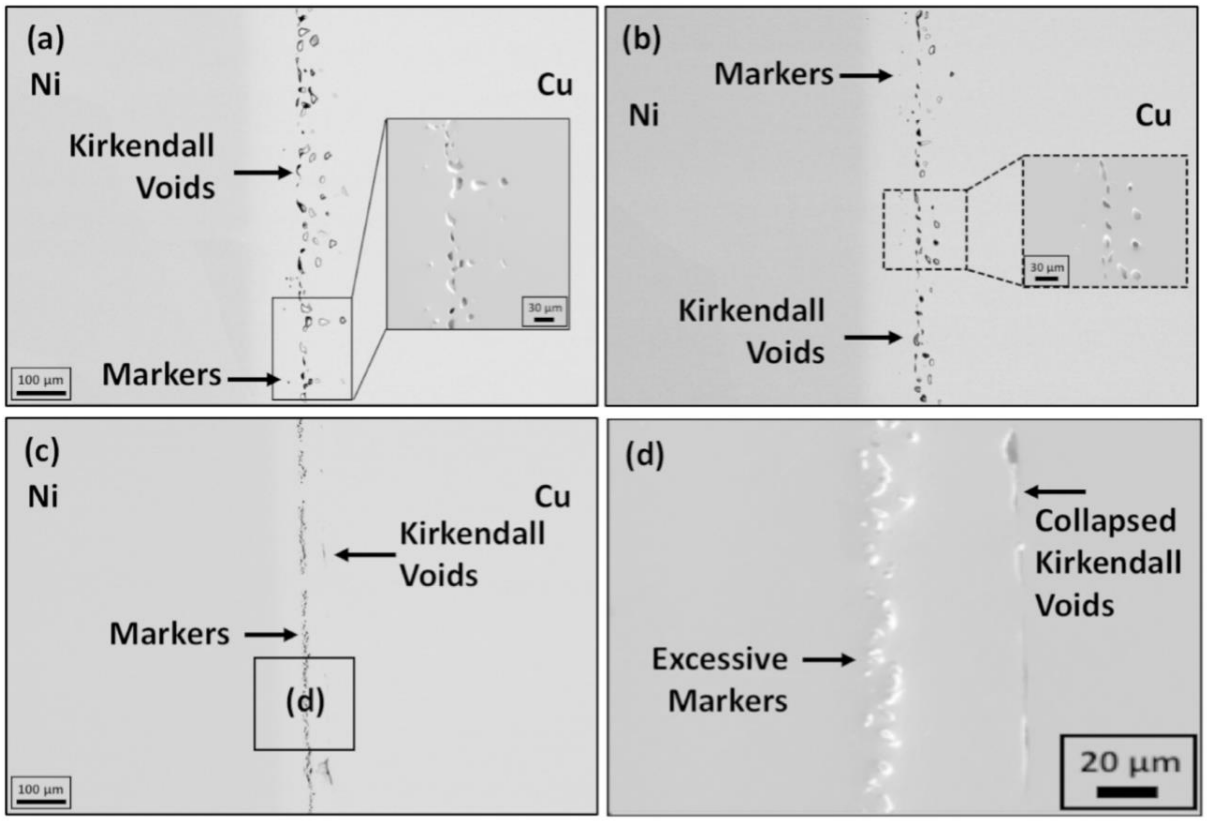

Figure 16 - Backscatter electron micrographs of Kirkendall voids development in the Cu vs. Ni diffusion couples annealed at 1000°C for 48 hours. Diffusion couples were assembled with 3-µm Al_2O_3 particle concentration (mg/ml) of (a) 0.67, (b) 5.00 (c,d) 33.33

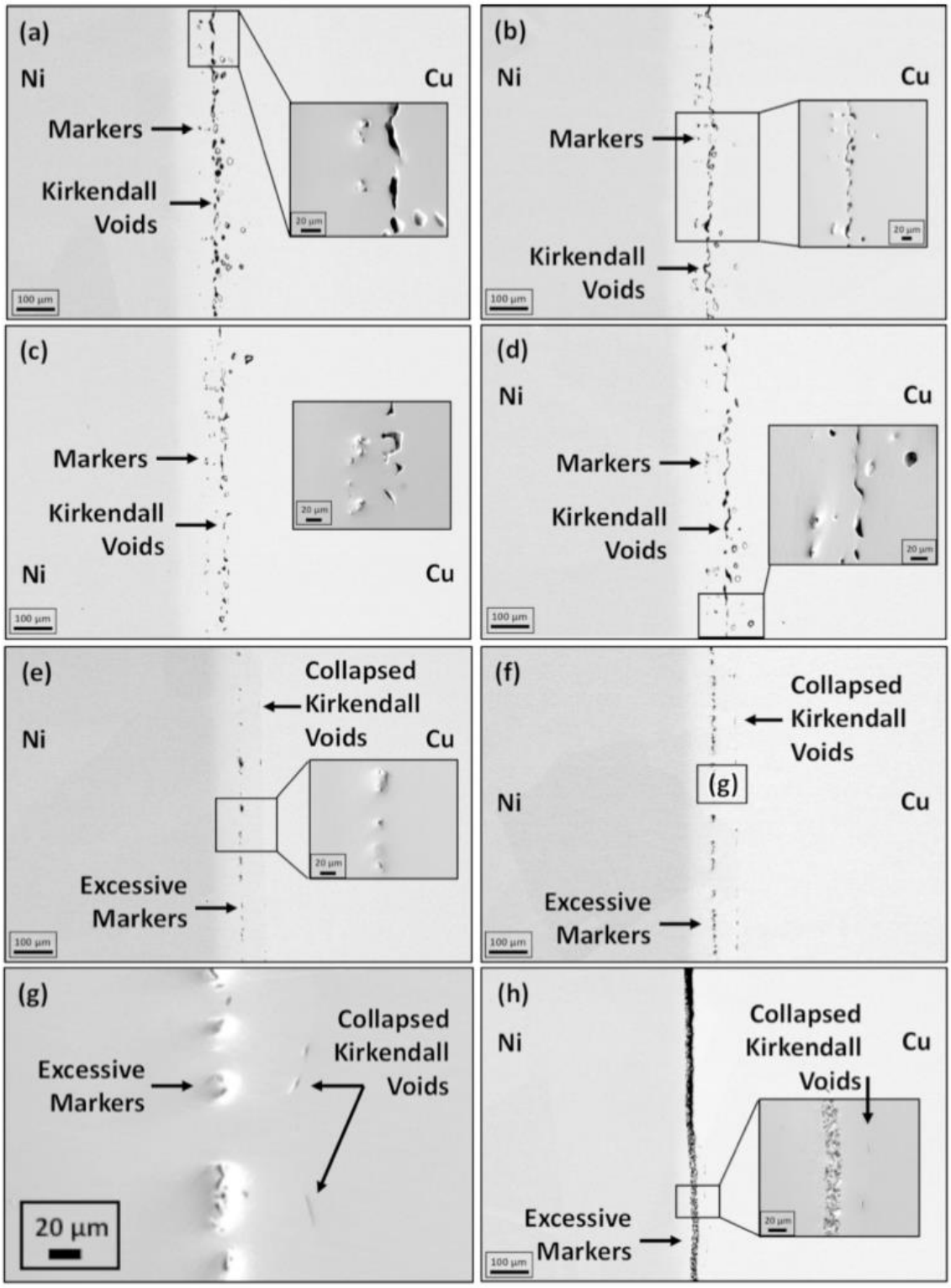
(a)
Ni
Cu
Markers
Kirkendall Voids
100 µm
20 µm
(b)
Ni
Cu
Markers
Kirkendall Voids
100 µm
20 µm
(c)
Markers
Kirkendall Voids
Ni
Cu
100 µm
20 µm
(d)
Ni
Cu
Markers
Kirkendall Voids
100 µm
20 µm
(e)
Collapsed Kirkendall Voids
Ni
Cu
Excessive Markers
100 µm
20 µm
(f)
Collapsed Kirkendall Voids
(g)
Ni
Cu
Excessive Markers
100 µm
(g)
Excessive Markers
Collapsed Kirkendall Voids
20 µm
(h)
Ni
Collapsed Kirkendall Voids
Cu
Excessive Markers
100 µm
20 µm

Figure 17 - Backscatter electron micrographs of Kirkendall voids development in the Cu vs. Ni diffusion couples annealed at 1000°C for 48 hours. Diffusion couples were assembled with 5-µm Al_2O_3 particle concentration (mg/ml) of (a) 0.67, (b) 1.67 (c) 3.33, (d) 4.00, (e) 5.00, (f,g) 6.67 and (h) 33.33.

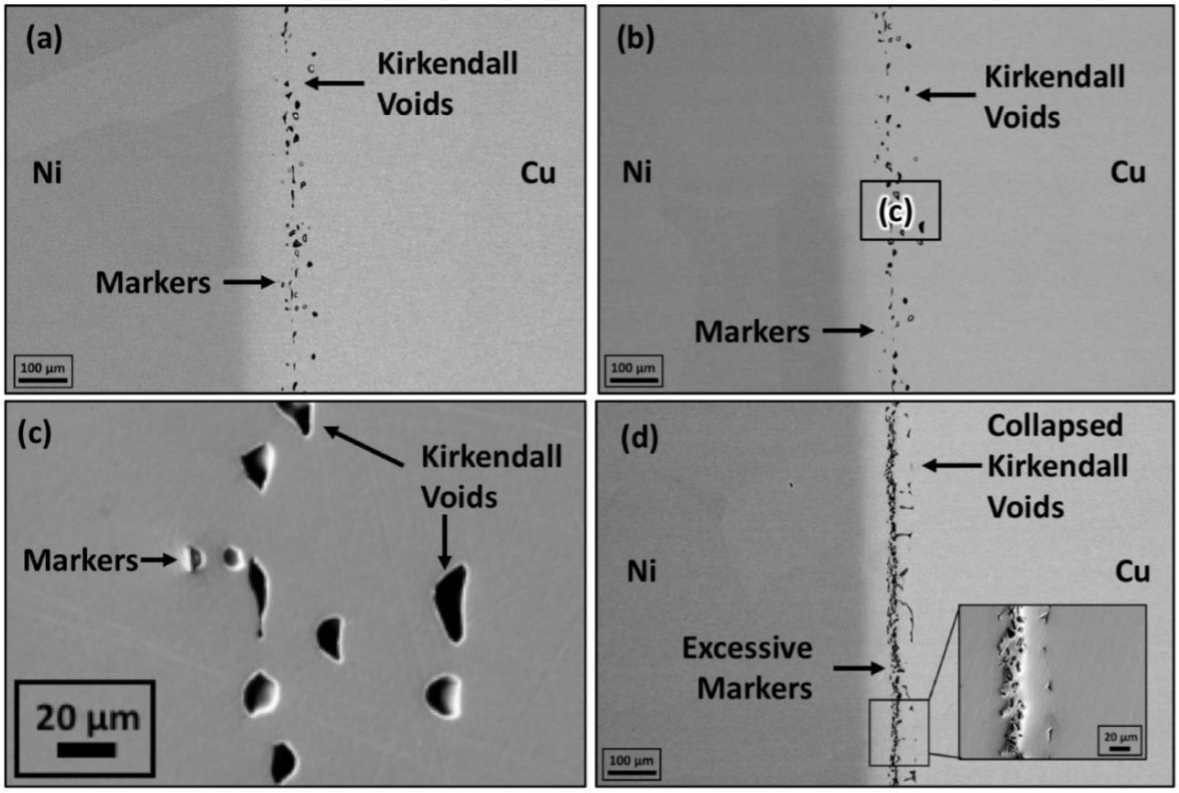

Figure 18 - Backscatter electron micrographs of Kirkendall voids development in the Cu vs. Ni diffusion couples annealed at 1000°C for 48 hours. Diffusion couples were assembled with 9-µm Al_2O_3 particle concentration (mg/ml) of (a) 0.67, (b,c) 5.00 (d) 33.33.

Extensive image analyses were carried out to quantitatively characterize these Kirkendall voids using the shape factor, f_1 as defined by Equation (39) Figure 19 presents the shape factor, f_1 measured from all diffusion couples examined in this study. Shape factor, f_1 increased as marker concentration increased for all couples. The magnitude of f_1 increased sharply with 1µm and 3-µm Al_2O_3 marker particles were employed with a concentration of 33.33 mg/ml as presented in Figure 19(a) and Figure 19(b). However, this sharp increase was not reported for 5-µm and 9-µm Al_2O_3 marker particles as shown in Figure 19(c) and Figure 19(d), because Kirkendall voids could not be distinguished as voids in backscatter electron micrographs that could be analyzed properly. In fact, one could mistakenly conclude that Kirkdendall voids do not exist in certain regions.

To elucidate the appearance of these "linear" features, an additional Cu vs. Ni diffusion couple, with 33.33 mg/ml of 3-µm Al_2O_3 marker particles, was annealed at 1000°C for 48 hours, and was furnace cooled. Figure 20(a) and Figure 20(b) presents secondary electron micrographs of diffusion couples that were water-quenched and furnace cooled, respectively. On the left side of these micrographs, markers are clearly presented. Upon furnace cooling, coalescence of Kirkendall voids into large gaps within the diffusion couple was observed as presented in Figure 20(b). The water-quenched couple clearly ended up with linear features as seen in Figure 20(a), which indicate that the coalesced voids collapsed (i.e., shear and compressive stress) during water-quenching. These collapsed gaps, unfortunately can be easily overlooked, particularly with smearing effect during metallographic preparation. They also explain the absence of an increase

in shape factor, f_1 in Figure 19(c) and Figure 19(d), because they were not discernable as voids for image analysis.

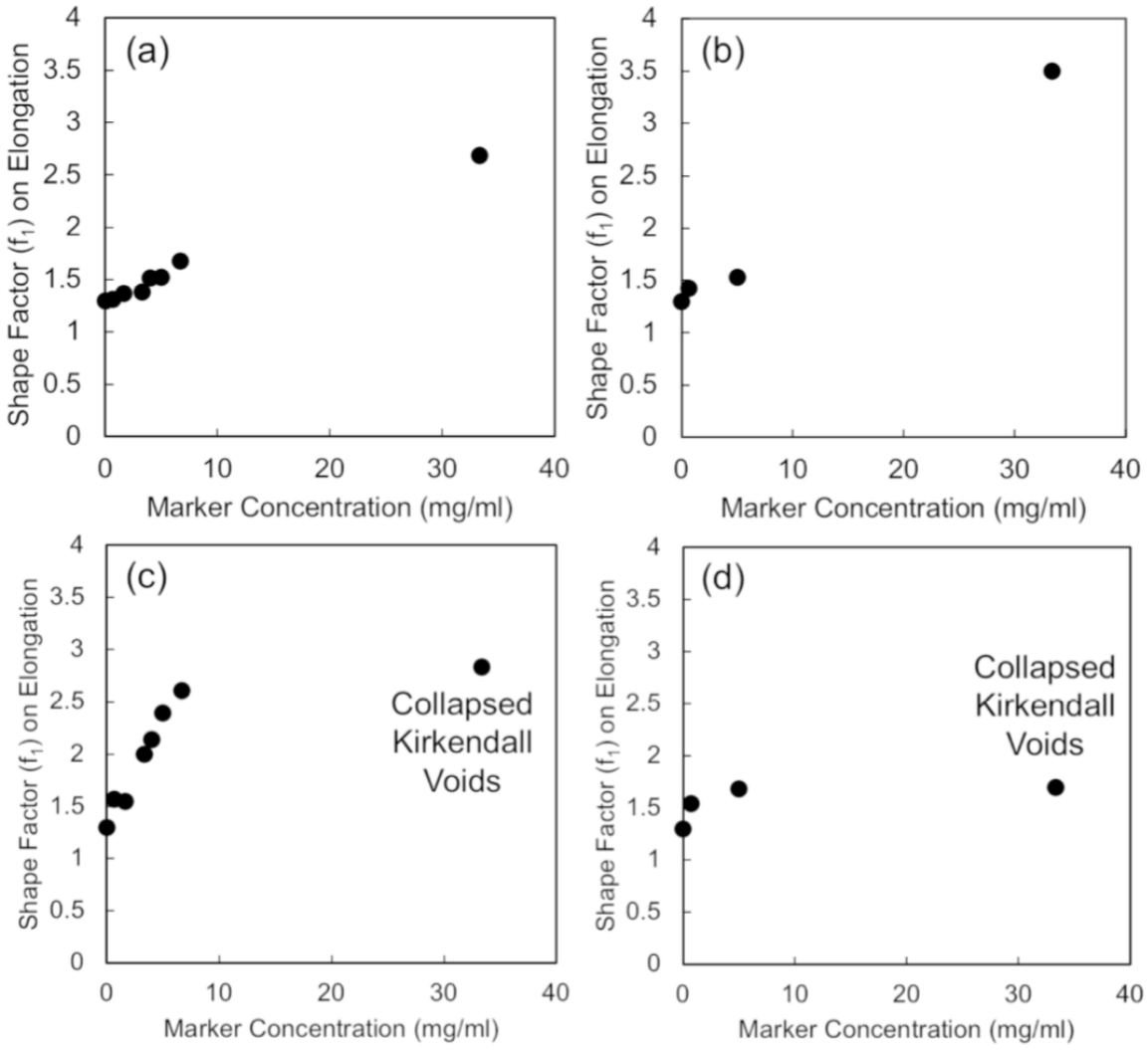

Figure 19 - Shape factor, f_1 on elongation of Kirkendall voids determined from Cu vs. Ni diffusion couples with varying concentration of Al_2O_3 marker particles, (a) 1 µm, (b) 3 µm, (c) 5 µm and (d) 9 µm in size.

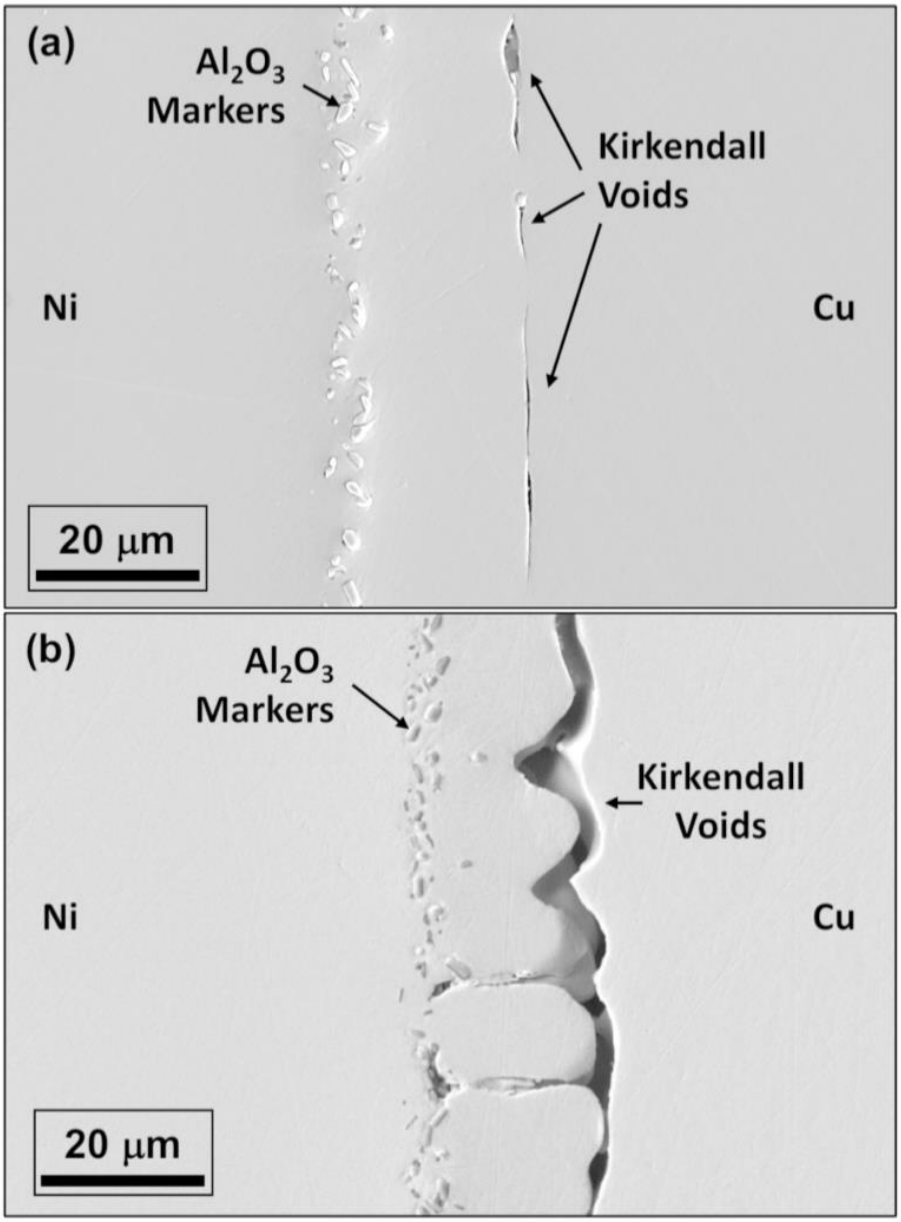

Figure 20 - Secondary electron micrographs of Kirkendall voids development in the Cu vs. Ni diffusion couple with 33.33 mg/ml of 5-μm Al_2O_3 marker particles. Diffusion couples were (a) water-quenched and (b) furnace cooled after annealed at 1000°C for 48 hours.

4.3 Interdiffusion Profile Analysis

Figure 21 presents a typical concentration profile of Cu determined by XEDS on FE-SEM from Cu vs. Ni diffusion couple annealed at 1000°C for 48 hours. Experimental data was fitted with Equation (38), and Boltzman-Matano Method was utilized for determining interdiffusion coefficient as a function of composition. After finding the location of the Matano plane (x_o), interdiffusion flux was calculated. Interdiffusion coefficient was obtained by combining Fick's law and with flux equations (Equation (10)).

The interdiffusion coefficients in the Cu vs Ni system at 1000°C was determined by Heumann and Grundhoff [35] and Iijima et al. [7] for the entire composition range. Interdiffusion coefficients determined by Iijima et al.[7] were slightly higher between 60 and 100 at. % of Cu. Figure 22 (a) shows the interdiffusion coefficients as a function of Cu composition for the couples #1, #4, and 7 (Cu75Ni-Cu50Ni-Cu-Cu75Ni) at 1000°C. Magnitude and composition dependence of interdiffusion coefficients obtained from these couples at 1000°C were in good agreement with those reported by Heumann and Grundhoff [35].

Tronsdal and Sørum [38] determined the temperature and concentration dependence of interdiffusion coefficients around 60 at.% Cu for the temperature range 700-1000°C. The interdiffusion coefficients reported by Trønsdal and Sørum [38] at 900°C and 800°C were significantly higher than the interdiffusion coefficients determined by this study as presented in Figure 22 (b) and (c). Hayashi et al. [39] also examined the Cu-Ni interdiffusion for the temperature range 760 and 910°C. The composition-dependence was similar; however, the magnitude of the interdiffusion coefficients was lower than those determined in this study.

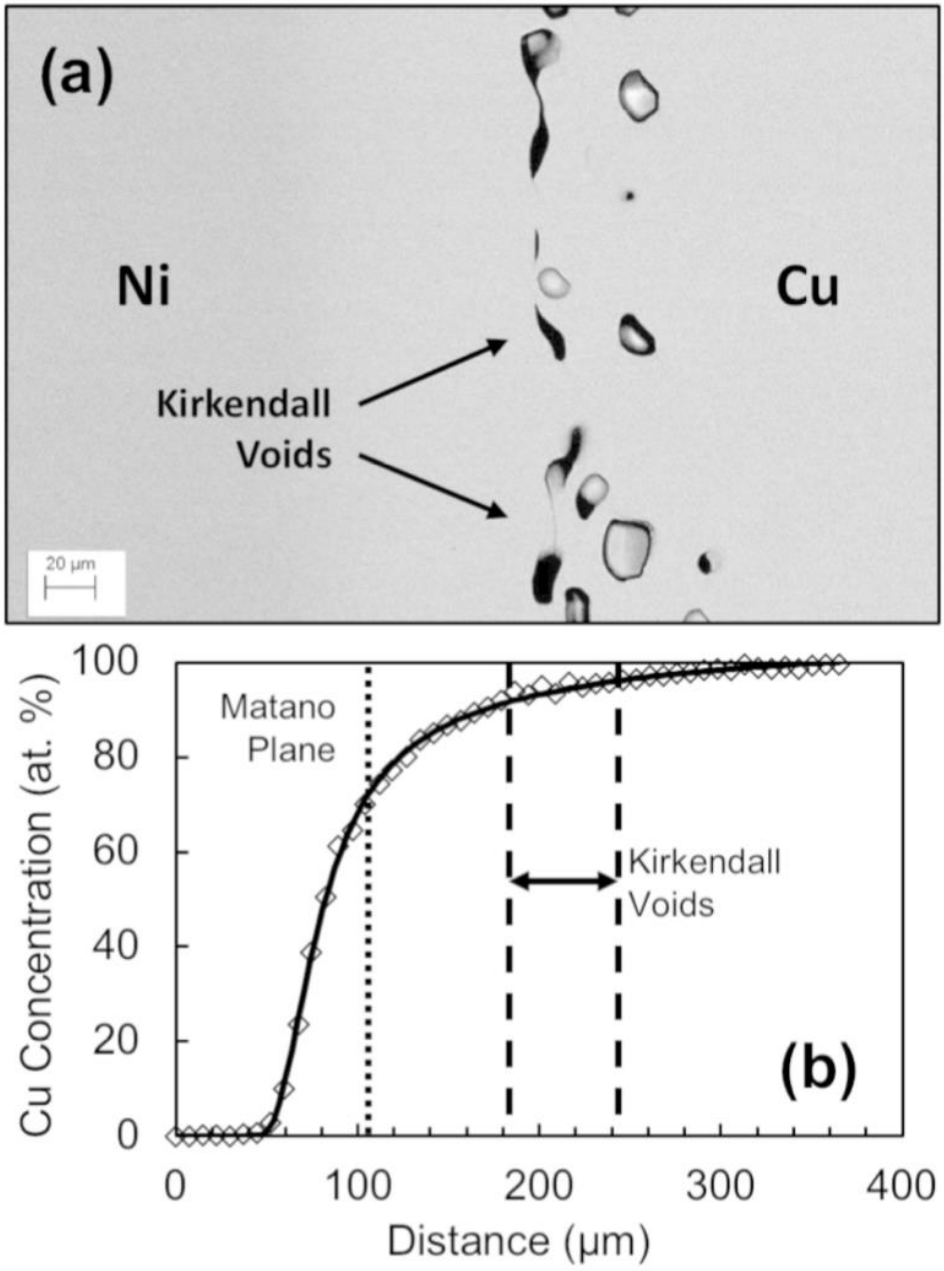

Figure 21 - (a) Backscatter electron micrograph and (b) the corresponding Cu concentration profile of Cu vs. Ni diffusion couple assembled with no markers.

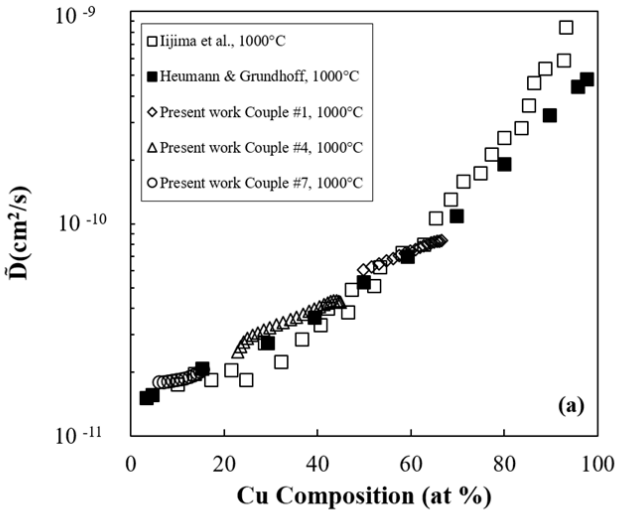
Iijima et al., 1000°C
Heumann & Grundhoff, 1000°C
Present work Couple #1, 1000°C
Present work Couple #4, 1000°C
Present work Couple #7, 1000°C
(a)
$\tilde{D}$(cm²/s)
Cu Composition (at %)

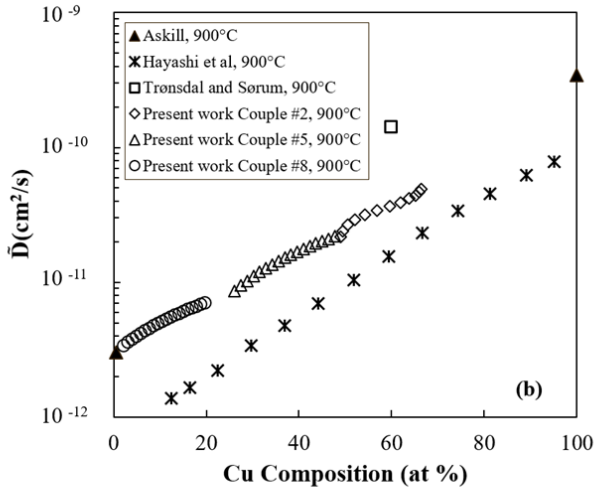
Askill, 900°C
Hayashi et al, 900°C
Trønsdal and Sørum, 900°C
Present work Couple #2, 900°C
Present work Couple #5, 900°C
Present work Couple #8, 900°C
(b)
$\tilde{D}$(cm²/s)
Cu Composition (at %)

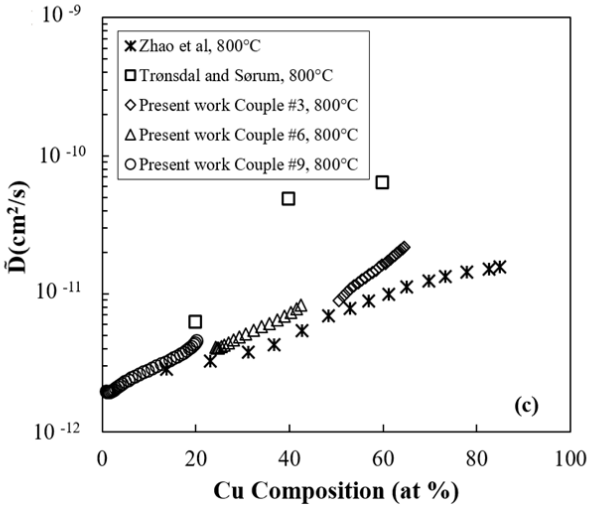
Zhao et al, 800°C
Trønsdal and Sørum, 800°C
Present work Couple #3, 800°C
Present work Couple #6, 800°C
Present work Couple #9, 800°C
(c)
$\tilde{D}$(cm²/s)
Cu Composition (at %)

Figure 22 – Interdiffusion coefficients determined as a function of Cu composition (at%) a) at 1000°C, b) 900°C c) 800°C.

In order to demonstrate that the magnitude and the trend of the interdiffusion coefficients' composition dependence obtained from this study were more consistent than Hayashi et al. and Tronsdal and Sørum, impurity diffusion coefficients reported by Askil [40] were also plotted in Figure 22(b)

Figure 22(c) presents study conducted by Zhao et al. [41] which they investigated interdiffusion coefficient of Cu and Ni in the temperature range of 650 and 850°C. Interdiffusion coefficients at 800°C at compositions 20 at.%, 40 at.% and 60 at.% Cu were also reported by Trønsdal and Sørum [38] and represented in Figure 22(c). Results obtained from this study demonstrate that the composition-dependence was consistent among all studies. However, the magnitude determined by this study falls between the values determined by Zhao et al.[41] and Trønsdal and Sørum [38].

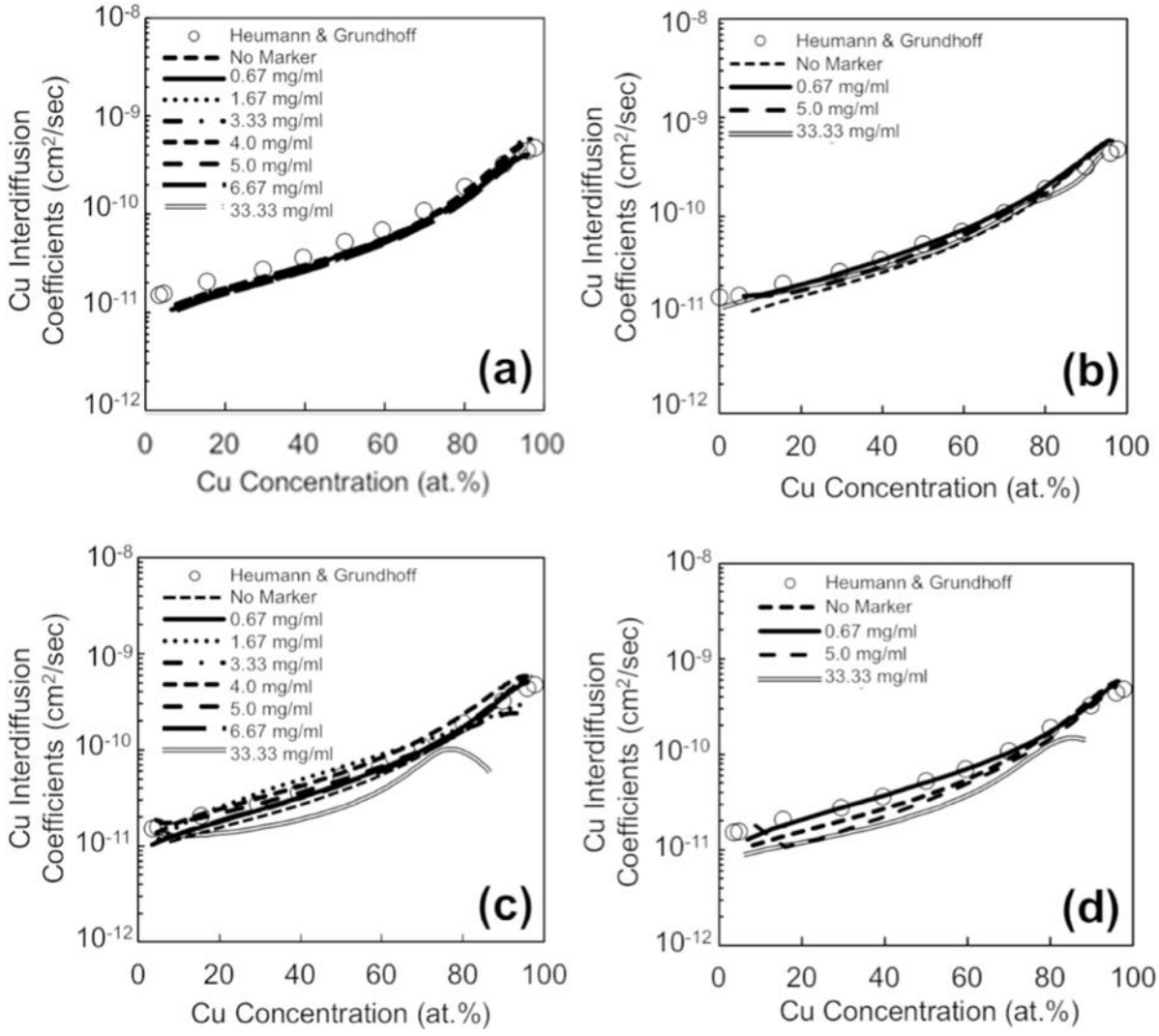

Figure 23 - Interdiffuson coefficient determined from the Cu vs. Ni diffusion couples annealed at 1000°C for 48 hours. Diffusion couples were assembled with varying concentration of Al_2O_3, (a) 1 µm, (b) 3 µm, (c) 5 µm and (d) 9 µm in size.

Figure 23 presents interdiffusion coefficients at 1000°C as a function of Cu concentration, determined from all diffusion couples containing Al_2O_3 markers in this study. Magnitude and composition-dependence of interdiffusion coefficients determined from couples with 1-µm and 3-µm Al_2O_3 marker particles were consistent with those reported by Heumann and Grundhoff [35]. However, deviation in both the magnitude and composition-dependence were observed from couples with 5-µm and 9-µm Al_2O_3 marker particles, particularly at a higher marker concentration of 33 mg/ml. In particular, a large deviation was observed at Cu concentration of 60 – 80 at.%. This composition range with a large deviation in interdiffusion coefficients corresponds to an excessive marker concentration, where a scatter in Cu concentration was observed, and collapsed gaps (e.g., from coalesced Kirkendall voids) where a "discontinuity" in Cu concentration was observed as presented in Figure 24

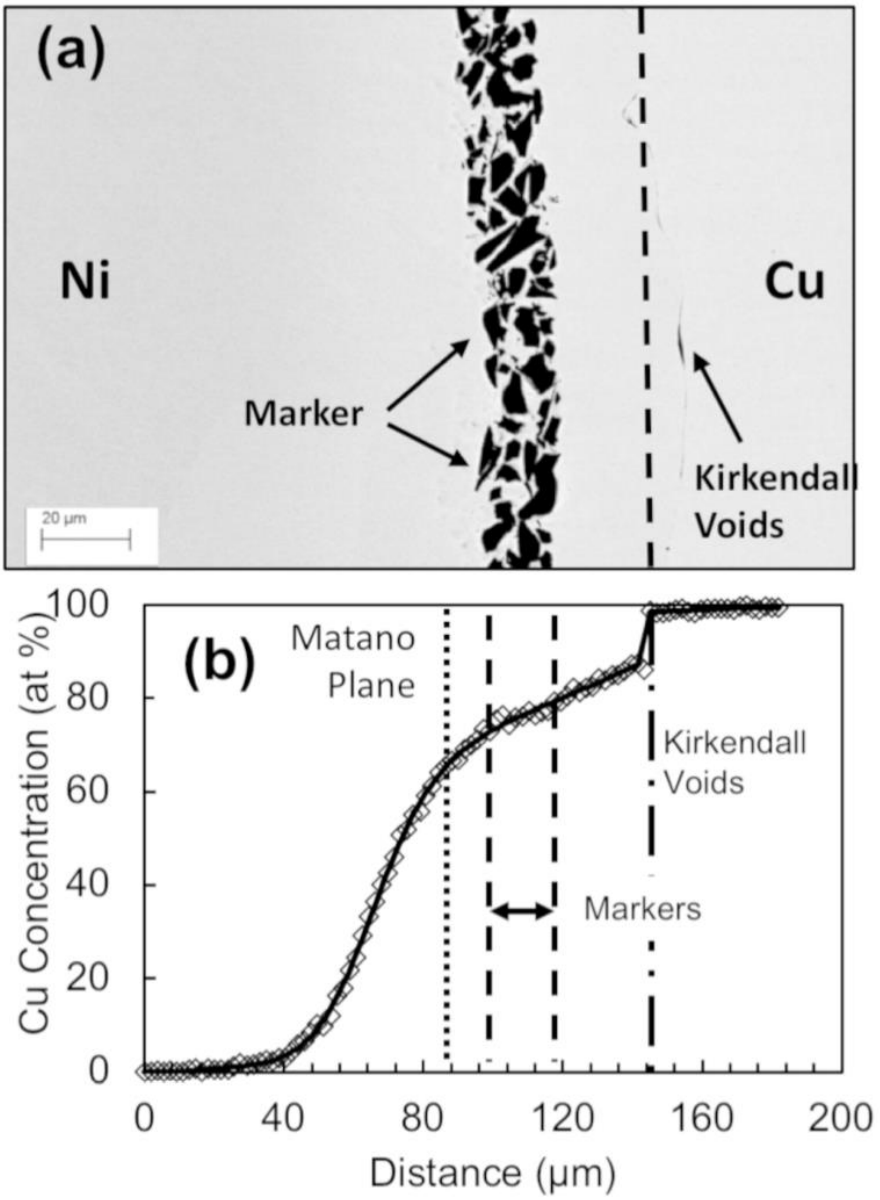

Figure 24 - *Backscatter electron micrograph and (b) the corresponding Cu concentration profile of Cu vs. Ni diffusion couple assembled with 33.33 mg/ml of 5-µm Al_2O_3 marker particles. Discontinuity in concentration profile from 80 to 100 at.% Cu corresponded to a location where collapsed Kirkendall voids were observed.*

4.4 Marker Movement and Intrinsic Diffusion

Marker composition and position relative to the Matano plane were measured as reported in Table 6. Figure 25 also presents the movement of markers relative to the Matano plane as a function of Al_2O_3 marker particles concentrations. For 1-µm and 3-µm Al_2O_3 marker particles, the movement did not vary up to 5.0 mg/ml marker concentration, which corresponds to, approximately, 23 percent areal coverage by the markers as presented in Table 5, Figure 10 and Figure 11. However a decrease in marker movement was observed with a higher maker concentration, particularly at 33 mg/ml as presented in Figure 25(a) and Figure 25(b).

For 5-µm and 9-µm Al_2O_3 marker particles, a decrease in marker movement was observed gradually as a function of marker concentration as presented in Figure 25(a) and Figure 25(b). Based on measured marker movement presented in Figure 25 and composition reported in Table 6, intrinsic diffusion coefficients of Cu was determined as presented in Figure 26. When compared to those reported by Heumann and Grundhoff [35], use of 1-µm and 3-µm Al_2O_3 particles as inert markers yielded consistent results in determining the intrinsic diffusion coefficients. However, a decrease in Cu intrinsic diffusion coefficients was observed with an increase in concentration of more than 0.67 mg/ml for 5-µm and 9-µm Al_2O_3 marker particles. The decrease in Cu intrinsic diffusion coefficients corresponded with the reduction in marker movement as indicated by the arrows in Figure 26(c) and Figure 26(d).

Table 6 – Matano plane and marker plane compositions from the Cu vs. Ni diffusion couples annealed at 1000°C for 48 hours.

Couple	Marker Size (μm)	Marker Concentration (mg/ml)	Matano Plane Composition* (at %)	Marker Plane Composition (at %)
1	No marker	0	69.9	N.A.
2	1	0.67	68.7	80.5 ± 0.9
3		1.67	69.4	81.6 ± 0.9
4		3.33	68.6	81.0 ± 0.9
5		4.00	69.7	81.5 ± 0.8
6		5.00	69.7	81.4 ± 0.8
7		6.67	69.3	81.8 ± 1.5
8		33.33	69.9	80.0 ± 1.2
9	3	0.67	69.5	80.5 ± 0.6
10		5.00	69.1	81.1 ± 0.9
11		33.33	69.6	78.2 ± 3.4
12	5	0.67	69.4	81.0 ± 0.6
13		1.67	69.3	81.2 ± 0.8
14		3.33	69.9	81.0 ± 0.6
15		4.00	69.3	79.3 ± 2.0
16		5.00	65.3	77.8 ± 0.9
17		6.67	63.7	77.3 ± 0.7
18		33.33	62.6	76.4 ± 2.3
19	9	0.67	68.4	80.8 ± 0.9
20		5.00	68.7	81.8 ± 0.9
21		33.33	65.2	76.9 ± 1.4

*Standard deviation of the Matano plane composition is 0.5 at%.

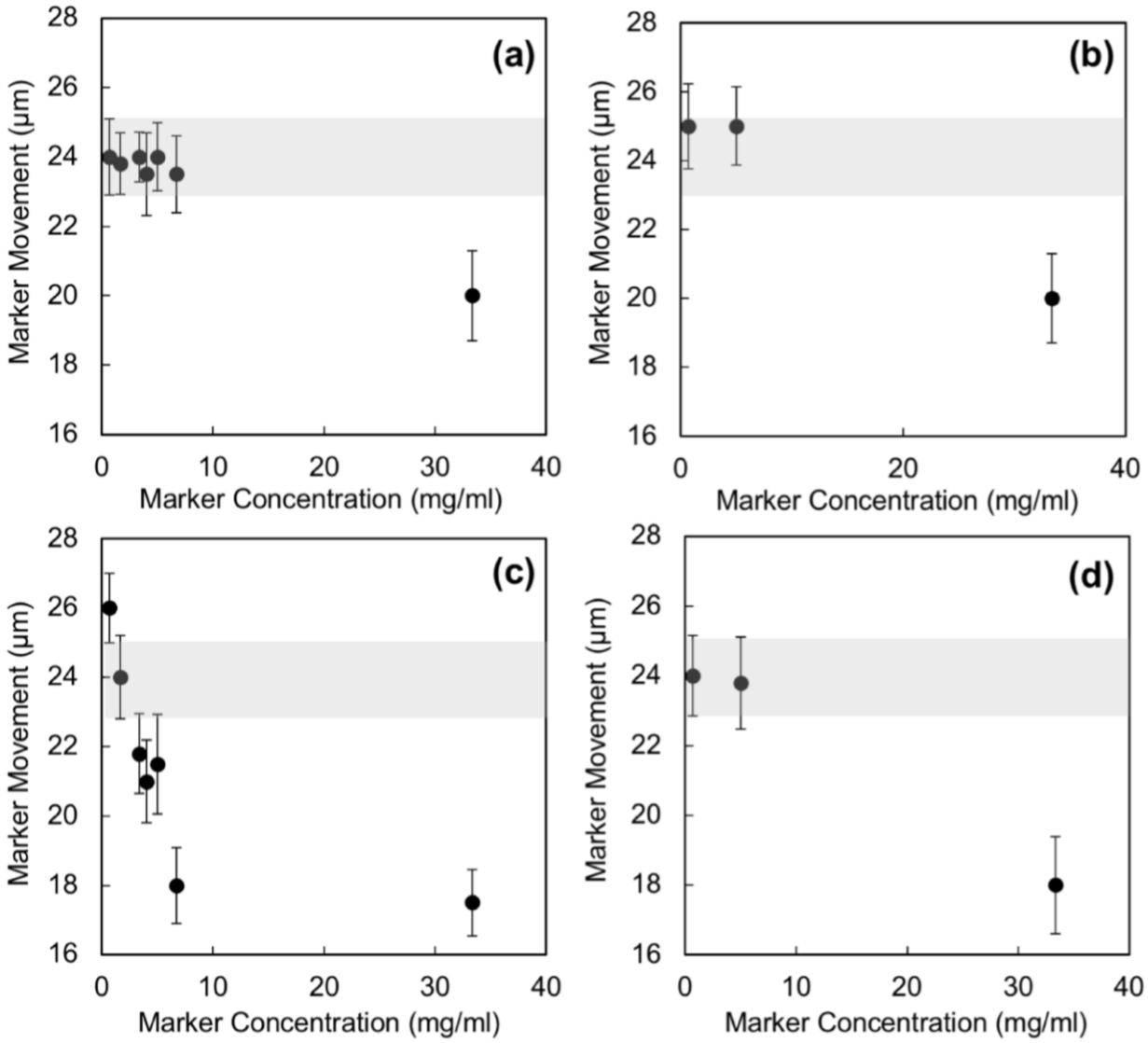

Figure 25 - Marker movement relative to the Matano plane in the Cu vs. Ni diffusion couples annealed at 1000°C for 48 hours, as a function of (a) 1 μm, (b) 3 μm, (c) 5 μm and (d) 9 μm Al_2O_3 marker particle concentration.

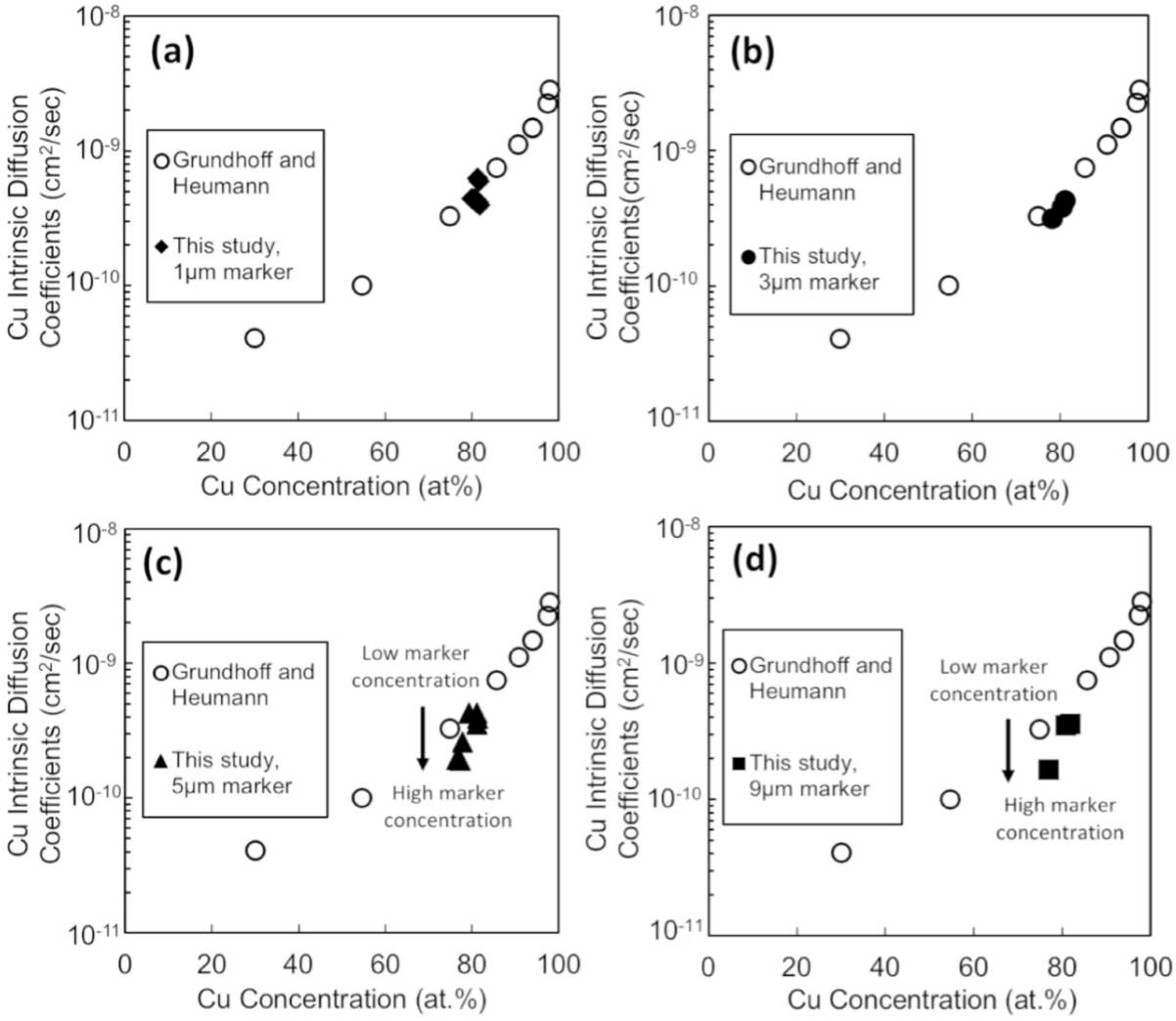

Figure 26 - Intrinsic diffuson coefficient of Cu determined from the Cu vs. Ni diffusion couples annealed at 1000°C for 48 hours as a function of (a) 1 μm, (b) 3 μm, (c) 5 μm and (d) 9 μm Al_2O_3 marker particle concentration.

4.5 Spike Profile Analysis

The prepared diffusion couple consists of both the standard interdiffusion part and part where the thin film sandwiched between two alloys as shown in Figure 3 As shown in the Figure 3, annealing of the diffusion couple creates a local spike in the composition of one of the alloy components (i.e., pure Cu thin film) which include contributions from both, interdiffusion and isotopic thin film diffusion. After annealing, the standard interdiffusion part and the sandwich part must be analyzed to provide both interdiffusion profiles. The analysis of the thin film profile (or spike profile) will give the total composition profile of Cu which includes the contributions from the standard interdiffusion profile and isotopic thin film profile. In order to obtain the c_{Cu1} profile, the interdiffusion contribution is subtracted from the total c_{Cu} profile. This way, separation of the fraction (i.e., c_{Cu2} fraction) of total Cu atoms (Equation (13) with A = Cu) and corresponding atomic fluxes as expressed by Equation (21) can be obtained. This approach of distinguishing thin film and interdiffusion profiles, i.e., Cu and Cu_2 profiles, is based on the assumption that the thickness of pure Cu layer is negligibly small. The subtraction was achieved by taking the mirror image of the interdiffusion profile and taking out c_{Cu2} profile from total c_{Cu} profile as demonstrated in Figure 27. Once the final, separated concentration profiles were obtained, Equation (37) was used to determine the tracer diffusion coefficient.

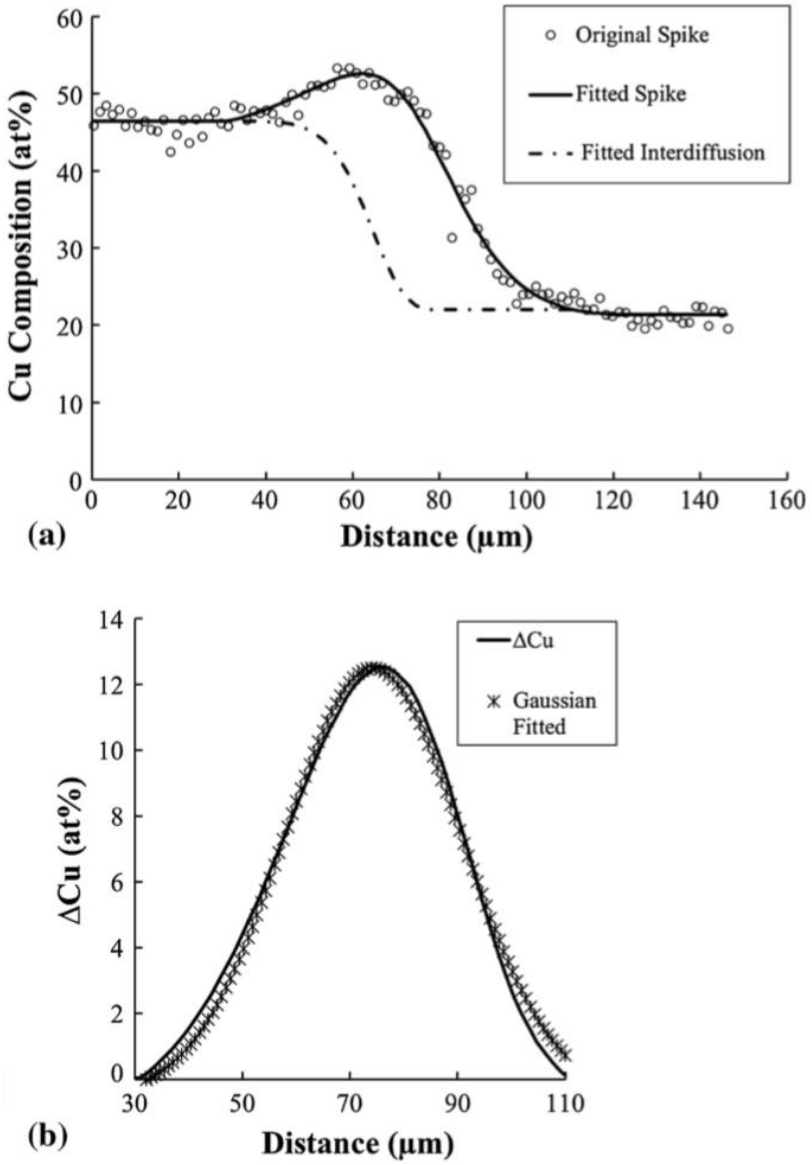

Figure 27 – (a) Concentration profile that includes both interdiffusion and thin film diffusion and (b) concentration profile from thin film diffusion extracted (ΔCu = Cu-Cu_2) and Gaussian distribution function

4.6 Tracer Diffusion Coefficient $\boldsymbol{D^*_{Cu}}$ at 800°C, 900°C, and 1000°C.

In Figure 28, tracer diffusion coefficient, D^*_{Cu} was determined based on the formalism developed by Belova et al [6] and plotted as a function of Cu composition near 50 at.%. As seen from the Figure 28, the application of the formalism successfully estimates the tracer diffusion coefficient of Cu, however, it does not give a reliable compositional dependence. Therefore, the tracer diffusion coefficient, D^*_{Cu} ,was also calculated utilizing the Gaussian distribution function applied to the c_{Cu1} profile and plotted against the corresponding spike composition without the full mathematical analysis. Table 7 summarizes the tracer diffusion coefficient, D^*_{Cu} obtained by application of the Belova *et* al. formalism as a function of Cu composition (at%) and the tracer diffusion coefficient calculated using Gaussian fitting function without the full mathematical analysis. When the existing literature tracer diffusion data obtained by radioactive isotopes studies [5] compared with the data obtained by this study utilizing Gaussian distribution function, an excellent agreement was found, as presented in Figure 29.

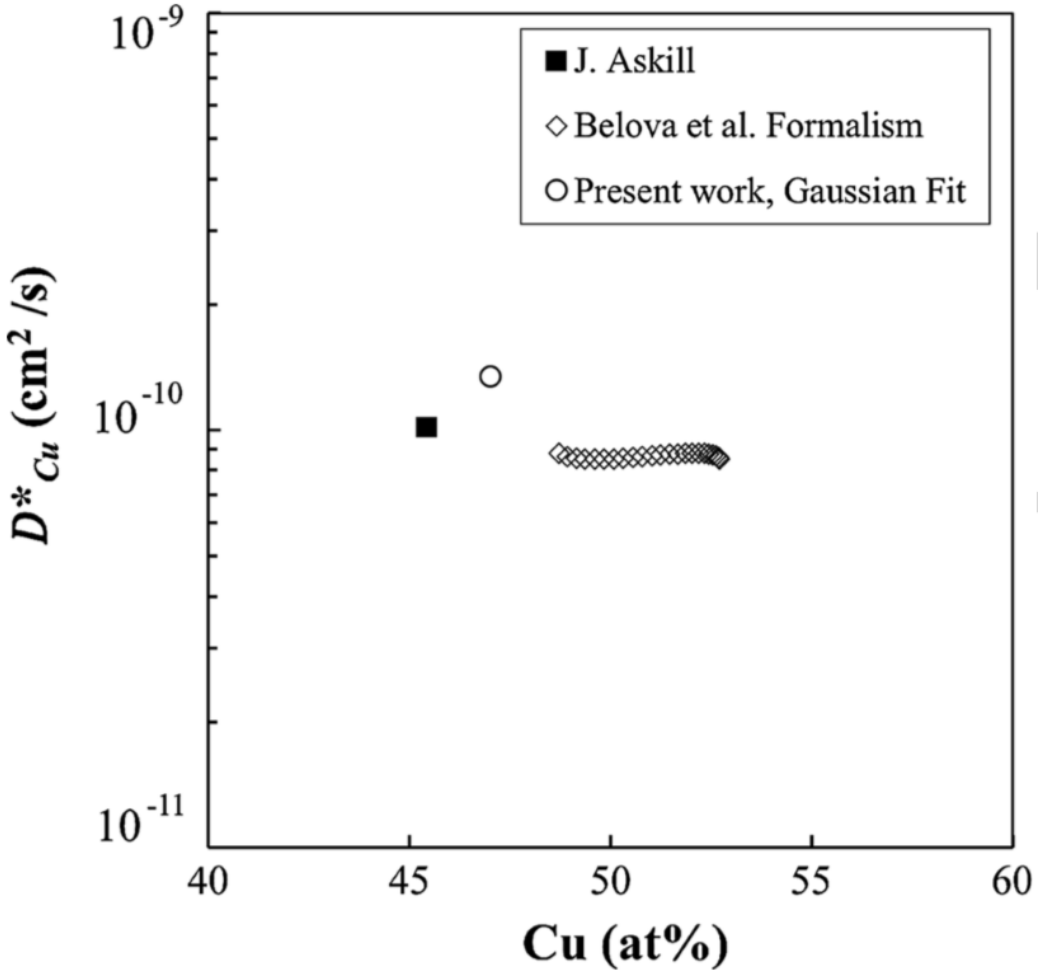

Figure 28 - Tracer diffusion coefficient, D^*_{Cu} determined by composition dependent analysis and Gaussian distribution function, independent of composition

Table 7 - Tracer diffusion coefficient derived from the Belova et al formalism and gaussian distribution function

Cu at %	D^*_{Cu} Belova et al. Formalism, cm^2/s	D^*_{Cu} Gaussian Distribution Function, cm^2/s
47	$8.6x10^{-11}$	$1.3x10^{-10}$
48	$8.6\ x10^{-11}$	
49	$8.6\ x10^{-11}$	
50	$8.6\ x10^{-11}$	

To further verify the applicability and consistency of the methodology, diffusion couples with varying terminal alloy compositions (Cu, Cu-25Ni, Cu-50Ni, Cu-75Ni, Ni) were annealed at 800, 900 and 1000°C, and analyzed for the simultaneous determination of tracer and interdiffusion coefficients as a function of composition.

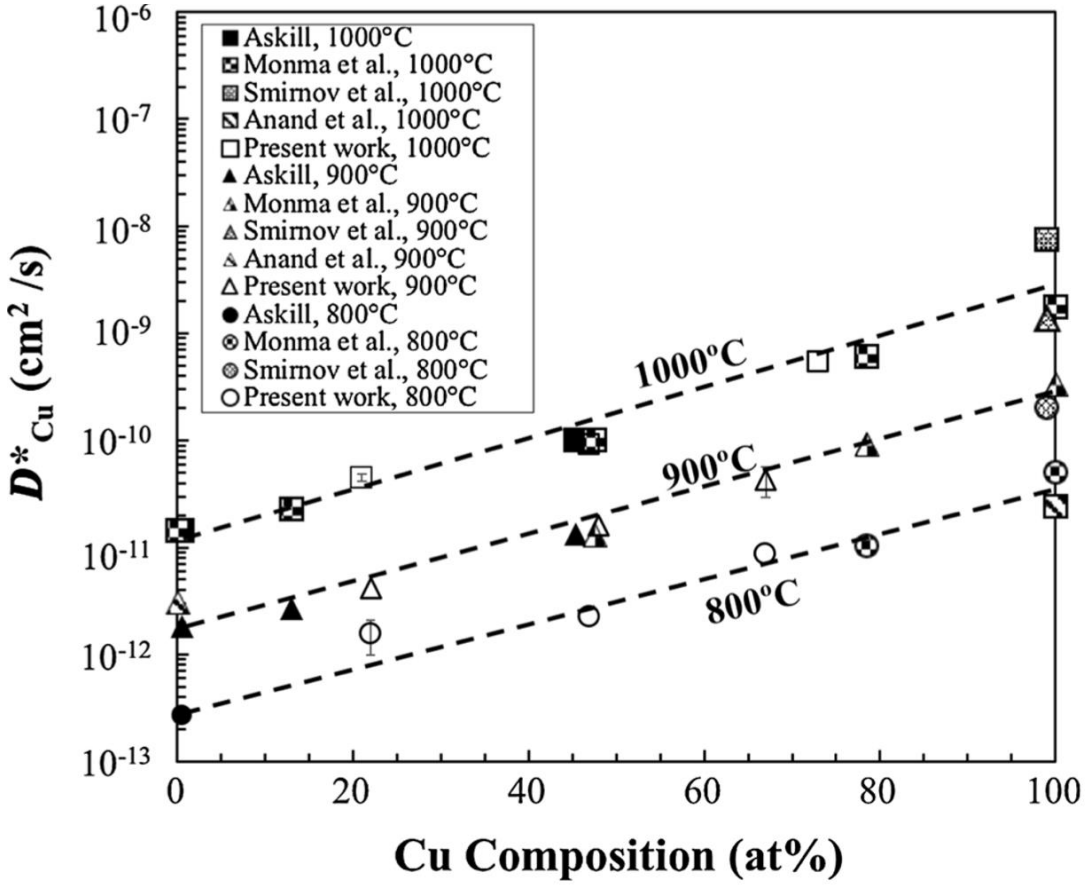

Figure 29 - Tracer diffusion coefficient, D^*_{Cu} determined as a function of composition based on Gaussian Distribution Function fitting of thin film diffusion

In order to determine the standard deviation for each temperature range and to demonstrate the repeatability of the experiments, independent diffusion couple experiments were also carried out, and corresponding standard deviations were determined. Denotations of ‘‘A’’ and ‘‘B’’ were used for the repeated couples. Table 8 summarizes the tracer diffusion coefficients, D^*_{Cu}, obtained from each diffusion couple examined in this study. Results from

1000°C, 900°C and 800°C were also compared to existing literature data [40, 42-44] obtained independently by radiotracer experiments as shown in Figure 29. It can be concluded that, in this investigation, the measurement of tracer diffusion coefficients in the Cu-Ni interdiffusion experimental set-up and utilizing the novel analytical framework produced reliable results. This study validates that this approach can be applied to other alloys as well to provide kinetic (i.e., tracer diffusion coefficients) and thermo-kinetic data (i.e., interdiffusion coefficients) from the same experiment without the use of radioactive or stable isotopes.

Table 8 - Summary of tracer diffusion coefficients obtained from each couple annealed

Couple	**Cu Composition (at %)**	**Temp (°C)**	**Time (sec)**	D^*_{Cu}**(cm^2/s)**	**Average D^*_{Cu}(cm^2/s)**	**Standard Deviation**
1	73	1000	900	$5.4\text{x}10^{-10}$	-	-
2-A	67	900	900	$5.7\text{x}10^{-11}$	$4.3\text{x}10^{-11}$	$7\text{x}10^{-12}$
2-B	67	900	900	$4.6\ \text{x}10^{-11}$		
3	67	800	5400	$8.0\text{x}10^{-12}$	-	-
4-A	47	1000	7200	$1.8\ \text{x}10^{-10}$	$1.4\ \text{x}10^{-10}$	$6\text{x}10^{-11}$
4-B	47	1000	7200	$9.0\ \text{x}10^{-11}$		
5	48	900	18000	$1.6\text{x}10^{-11}$	-	-
6	47	800	75600	$2.5\text{x}10^{-12}$	-	-
7-A	21	1000	3600	$4.1\text{x}10^{-11}$	$4.5\text{x}10^{-11}$	$4\text{x}10^{-12}$
7-B	21	1000	3600	$4.9\ \text{x}10^{-11}$		
8	22	900	3600	$4.2\text{x}10^{-12}$	-	-
9-A	22	800	10800	$9.9\text{x}10^{-13}$	$8.7\text{x}10^{-13}$	$2\text{x}10^{-13}$
9-B	22	800	10800	$7.5\text{x}10^{-13}$		

4.7 Tracer Diffusion Coefficient D^*_{Ni} at 800°C, 900°C, and 1000 °C

To further verify the applicability and consistency of the methodology, diffusion couples prepared with Ni thin film with varying terminal alloy compositions were annealed at 800°C, 900°C and 1000°C, and analyzed for the simultaneous determination of tracer and interdiffusion coefficients as a function of composition. Tracer diffusion coefficient, D^*_{Ni} was determined using Gaussian distribution function and plotted over the spike composition as shown in Figure 30.

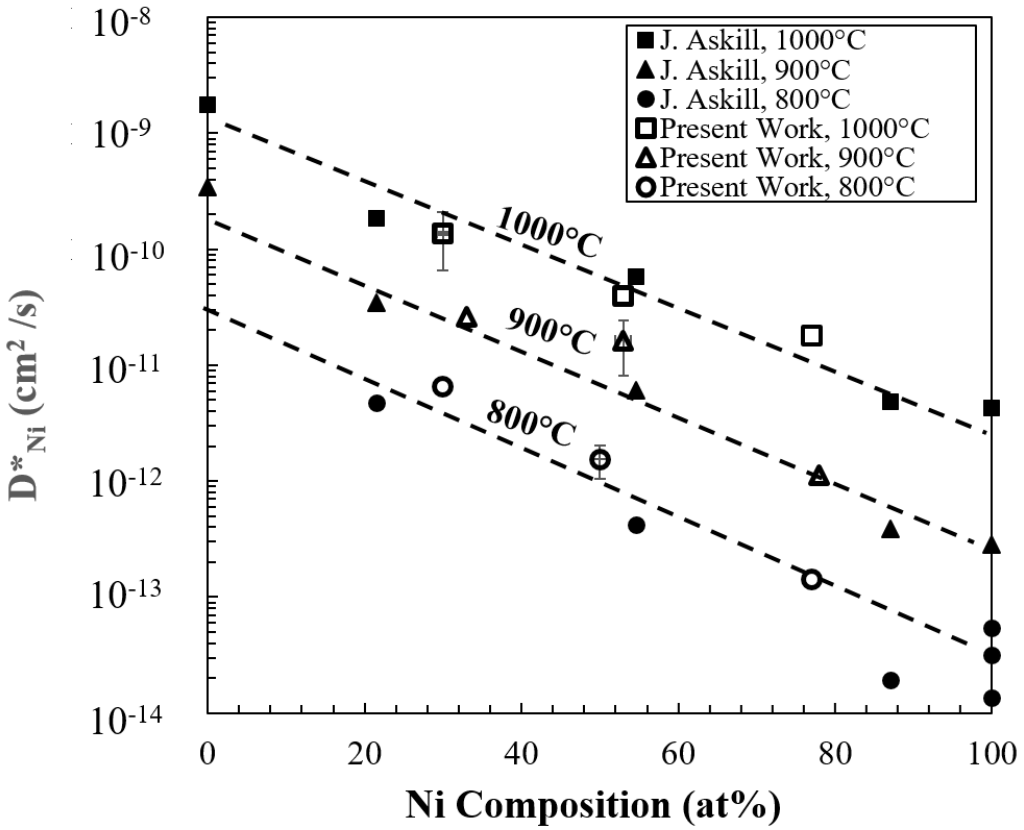

Figure 30 - Tracer diffusion coefficient, D^*_{Ni} determined as a function of composition based on Gaussian distribution function fitting of thin film diffusion

4.8 Interdiffusion Coefficient $\widetilde{\boldsymbol{D}}_{\mathrm{Ni}}$ calculated using Darken-Manning Relation at 1000°C

As mentioned previously, in binary systems, the Darken-Manning equation relates the interdiffusion coefficient $\widetilde{D}$, to mole fractions (X_A and X_B) , tracer diffusion coefficients D_A^* and D_B^*, thermodynamic factor and vacancy wind factor [22]. In Equation (40) ,$\emptyset$ is the thermodynamic factor and S is the vacancy wind factor. Generally, the vacancy wind factor is ignored assuming its contribution is small.

$$\widetilde{D} = (X_B . D_A^* + X_A . D_B^*) S\emptyset \qquad (40)$$

Based on Equation (40), interdiffusion coefficient was calculated using the calculated tracer diffusion coefficient for Cu, Ni, and thermodynamic factor from the literature. The thermodynamic factor at 1000°C was taken as 0.52, 0.4,and 0.50 at the concentrations 25, 50 and 75 respectively (Figure 31) [45]. As seen in the Figure 32, estimation of interdiffusion coefficient from calculated tracer diffusion coefficients was also produced agreeing values with the literature.

Table 9 – Interdiffusion Coefficient $\widetilde{\boldsymbol{D}}_{Ni}$ calculated using Darken-Manning Relation

Ni (at %)	$\boldsymbol{D^*_{Ni}}$	$\boldsymbol{D^*_{Cu}}$	**Ø**	$\boldsymbol{\widetilde{D}}$	$\boldsymbol{\widetilde{D}_{lit}}$
25	$1.80x10^{-11}$	$4.13x10^{-11}$	0.52	$\mathbf{1.04}x10^{-10}$	$\mathbf{1.08}x10^{-10}$
50	$3.94\ x10^{-11}$	$1.4\ x10^{-11}$	0.41	$\mathbf{3.67}\ x10^{-11}$	$\mathbf{3.60}\ x10^{-11}$
75	$6.54\ x10^{-11}$	$5.42\ x10^{-10}$	0.50	$\mathbf{1.87}\ x10^{-11}$	$\mathbf{2.06}\ x10^{-11}$

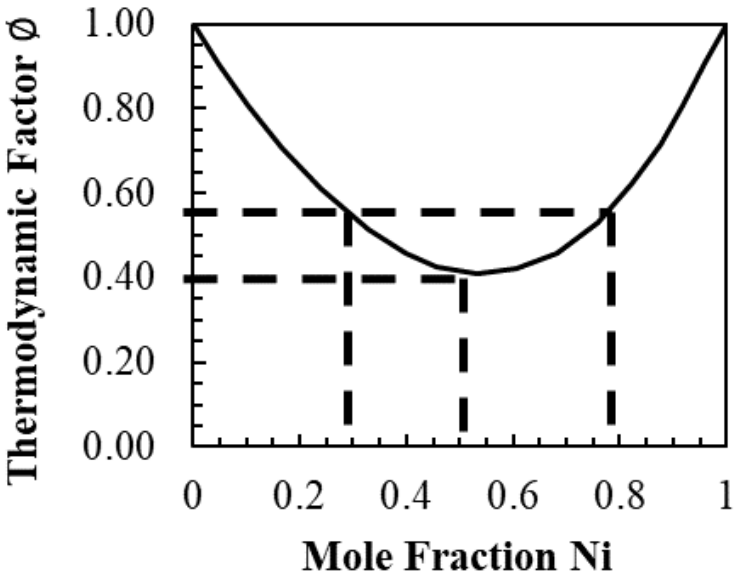

Figure 31 – Calculated thermodynamic factor Ø of the fcc phase in the Cu-Ni system at 1000°C [45]

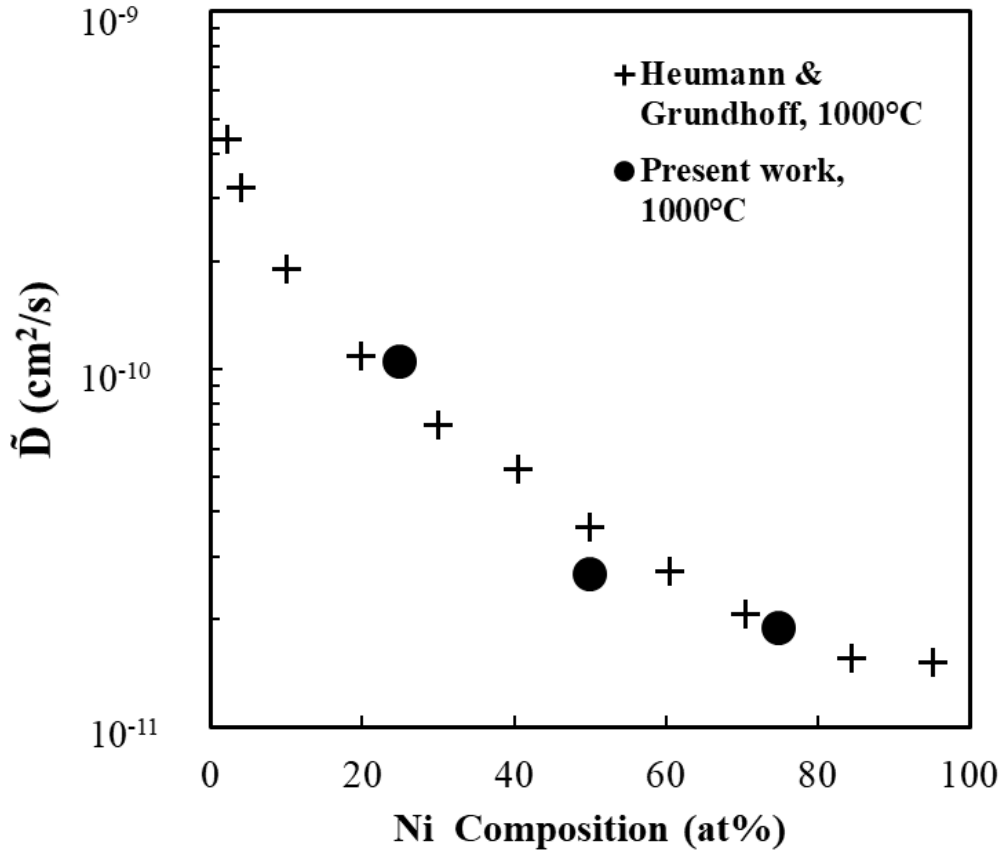

Figure 32 – Interdiffusion coefficient $\widetilde{D}_{Ni}$ calculated using Darken-Manning Relation at 1000°C.

CHAPTER 5 DISCUSSION

5.1 Effect of Markers on Interdiffusion and Intrinsic Diffusion

Inert markers employed in diffusion study, ultimately have to be observed easily and consistently on the cross-section of the diffusion couple, without influencing the process of diffusion, i.e., unidirectional and unobstructed diffusional flux. Findings from this investigation clearly demonstrate that the size and the amount of makers employed in diffusion couple study can influence the magnitude of interdiffusion and intrinsic diffusion coefficients. For the Cu-Ni system examined with Al_2O_3 particle markers ranging from 1 to 9 μm in size, the 1-μm and 3μm Al_2O_3 marker particles with concentration no more than 5 mg/ml were observed to yield consistent results with negligible deviation in diffusion coefficients determined. However, the 1-μm Al_2O_3 marker particles can be challenging to locate, for example by optical microscopy, with insufficient amount, and tend to agglomerate significantly as shown in Figure 10. For 5-μm and 9-μm Al_2O_3 marker particles, only the concentration of 0.67 mg/ml was acceptable to yield consistent interdiffusion and intrinsic diffusion coefficients. Based on optical micrographs of Ni surface prior to the diffusion couple assembly, these results correspond to areal coverage of no more than 20 percent for 1-μm and 3-μm Al_2O_3 marker particles, and 10 percent for 5-μm and 9-μm Al_2O_3 marker particles.

This study also can be extended to provide an important insight for the surface modification and coatings technology. In cases where surface modification and coatings produce metal-to-metal or alloy-to-alloy contact, presence of excessive oxide scale can have a significant

impact on the microstructural development including the coalescence of Kirkendall voids. Formation of voids is undesirable in most load-bearing circumstances, but the coalescence of voids into gaps, normal to the direction of diffusional flux, as observed in this study, would significantly undermine the integrity of surface modification and coatings, particularly under tensile and shear loading.

5.2 Simultaneous Measurement of Tracer Diffusion Coefficients and Interdiffusion Diffusion Coefficients

As shown in the Figure 28, the Belova et al [6] formalism successfully estimated the tracer diffusion coefficient of Cu however, it did not give a reliable compositional dependence. Therefore, the tracer diffusion coefficient, D_{Cu}^{*} ,was also calculated utilizing the Gaussian distribution function applied to the c_{Cu1} profile without the full mathematical analysis. When the existing literature tracer diffusion data obtained by radioactive isotopes studies compared with the data obtained by this study utilizing Gaussian distribution function, results showed that simple Gaussian distribution function application to the processed concentration profiles could be an efficient and convenient way for measuring tracer diffusion coefficients.

CHAPTER 6 CONCLUSION

6.1 Effects of marker size and distribution on the development of Kirkendall voids, interdiffusion coefficients, marker plane movement and intrinsic diffusion coefficients

Effects of marker size and distribution on the development of Kirkendall voids, interdiffusion coefficients, marker plane movement and intrinsic diffusion coefficients were studied using Cu vs. Ni solid-to-solid diffusion couple annealed at 1000°C for 48 hours. The Al_2O_3 particle markers ranged from 1 to 9 μm in size, and its distribution was varied by varying the amount dispersed in absolute ethanol from 0.67 to 33.33 mg/ml, which corresponded to cross-sectional coverage from 4 to 90 percent, approximately. Findings from this investigation are:

1. As the marker concentration (or areal coverage) increased, the Kirkendall voids became more interconnected and elongated. Extreme case of interconnection and elongation of Kirkendall voids produced "gaps" within the interdiffusion zone, which was observed to collapse during water-quenching. This "gap" also corresponded to a development of discontinuity in concentration profiles.

2. The 1-μm and 3-μm Al_2O_3 marker particles with concentration no more than 5 mg/ml were observed to yield consistent results with negligible variation in interdiffusion and intrinsic diffusion coefficients. For 5-μm and 9-μm Al_2O_3 marker particles, only the concentration of 0.67 mg/ml was acceptable to yield consistent interdiffusion and intrinsic diffusion coefficients.

3. These results correspond to the coverage of cross-section area normal to the diffusional flux no more than 23 percent for 1-μm and 3-μm Al_2O_3 marker particles, and no more than 11 percent for 5-μm and 9-μm Al_2O_3 marker particles.

6.2 Simultaneous Measurement of Tracer Diffusion Coefficients and Interdiffusion Diffusion Coefficients

The tracer diffusion coefficient, D^*_{Cu} and inter-diffusion coefficients simultaneously determined using the experimental methodology based on the new formalism and Gaussian distribution function from ordinary diffusion couple experiments without using any radioactive or stable isotopes. Results produced were in excellent agreement with previously reported values determined independently by radiotracer and other inter-diffusion experiments. Results showed that the new formalism can be applied successfully to binary systems without using radiotracers and self/tracer diffusivities can be obtained from traditional diffusion couple experiments.

In case of the faster diffusing atoms (Cu), the Belova et al. formalism gave an average estimation for the tracer diffusion coefficient, but not a reliable composition dependence. Therefore, Gaussian distribution function was also utilized to determine tracer diffusion coefficients, $D^*_{Cu}$and D^*_{Ni} and compared with the literature. Results showed that simple Gaussian distribution function application to the processed concentration profiles could be an efficient and convenient way for measuring tracer diffusion coefficients.

If the inert marker shift is also measured, in principle, all diffusion coefficients (tracer and intrinsic) may be determined in the same experiment, though the intrinsic diffusion coefficients would be measurable only at the composition of the marker plane.

CHAPTER 7 FUTURE WORK

This study should be extended to further to multi-component diffusion couples such as High Entropy Alloys (HEA). These alloys are currently the focus of significant attention in materials science and engineering because they have potentially desirable properties. Furthermore, research indicates that some HEAs have considerably better strength-to-weight ratios, with a higher degree of fracture resistance, tensile strength, as well as corrosion and oxidation resistance than conventional alloys [46].

Rigorous analysis of the interdiffusion experiments becomes more and more sophisticated for three and more elements in an alloy and it is challenging to derive physically sound quantities from traditional multicomponent diffusion experiments. Tracer diffusion coefficients are already being measured dominantly for polycrystalline and in some cases for single crystalline high-entropy alloys. However, the radiotracer technique is usually utilized in to access to the tracer diffusion coefficients in these alloys.

This study shows that the Gaussian distribution function application to the obtained concentration profiles can be implemented into multicomponent alloys including high entropy alloys to determine tracer diffusion coefficients and should be the concentration of the future work.

LIST OF REFERENCES

1. Manning, J.R., *Correlation Factors for Diffusion in Nondilute Alloys.* Physical Review B, 1971. **4**(4): p. 1111-1121.

2. Shewmon, P.G., *Diffusion in solids*. 1989: Warrendale, Pa. : Minerals, Metals & Materials Society, c1989. 2nd ed.

3. DeHoff, R.T. and K. Nagraj, *The Trouble with Diffusion.* Materials Research, Vol 5, Iss 3, Pp 209-229 (2002), 2002(3): p. 209.

4. Borgenstam, A., et al., *DICTRA, a tool for simulation of diffusional transformations in alloys.* Journal of Phase Equilibria, 2000. **21**(3): p. 269.

5. Benninghoven, A., F.G. Rudenauer, and H.W. Werner, *Secondary ion mass spectrometry: basic concepts, instrumental aspects, applications and trends*. 1987.

6. Belova, I.V., Y.H. Sohn, and G.E. Murch, *Measurement of tracer diffusion coefficients in an interdiffusion context for multicomponent alloys.* Philosophical Magazine Letters, 2015. **95**(8): p. 416-424.

7. Iijima, Y., K.-i. Hirano, and M. Kikuchi, *Determination of Intrinsic Diffusion Coefficients in a Wide Concentration Range of a Cu–Ni Couple by the Multiple Markers Method.* Transactions of the Japan Institute of Metals, 1982. **23**(1): p. 19-23.

8. van Dal, M.J.H., et al., *Intrinsic diffusion and Kirkendall effect in Ni–Pd and Fe–Pd solid solutions.* Acta Materialia, 2000. **48**(2): p. 385-396.

9. Belova, I.V. and G.E. Murch, *Phenomenological coefficients in solid-state diffusion*. 2016, Universitätsbibliothek Leipzig.

10. Kauffman, G.B., *Ullmann's Encyclopedia of Industrial Chemistry*. Journal of College Science Teaching, 2001(7): p. 491.

11. Paul, A., et al., *Atomic Mechanism of Diffusion.* Thermodynamics, Diffusion & the Kirkendall Effect in Solids, 2014: p. 167.

12. Faupel, F., et al., *Diffusion in metallic glasses and supercooled melts.* Reviews of modern physics, 2003. **75**(1): p. 237.

13. Wilson, R.G., F.A. Stevie, and C.W. Magee, *Secondary ion mass spectrometry : a practical handbook for depth profiling and bulk impurity analysis*. 1989: New York : Wiley, c1989.

14. De Souza, R.A. and M. Martin, *Secondary ion mass spectrometry (SIMS) - a powerful tool for studying mass transport over various length scales.* Physica Status Solidi (C), 2007. **4**(6): p. 1785.

15. Le Claire, A.D., *Solute diffusion in dilute alloys.* Journal of Nuclear Materials, 1978. **69**(Supplement C): p. 70-96.

16. Mehrer, H., *Diffusion in solids: fundamentals, methods, materials, diffusion-controlled processes*. Springer Series in Solid-State Sciences: 155. 2007. 212.

17. Fick, A., *V. On liquid diffusion.* Philosophical Magazine Series 4, 1855. **10**(63): p. 30-39.

18. Glicksman, M.E., *Diffusion in solids*. 2000: Wiley.

19. Darken, L.S., *Diffusion, Mobility and Their Interrelation through Free Energy in Binary Metallic System.* Trans. Am. Inst. Mining Metall. Eng., 1948. **175**: p. 184.

20. Hartley, G.S., *Diffusion and swelling of high polymers. Part I.—The swelling and solution of a high polymer solid considered as a diffusion process.* Transactions of the Faraday Society, 1946. **42**: p. B006.

21. Manning, J.R. and L. Bruner, *Diffusion kinetics for atoms in crystals.* American Journal of Physics, 1968. **36**(10): p. 922-923.

22. Paul, T.R., et al., *Determining a Tracer Diffusivity by way of the Darken-Manning Equation for Interdiffusion in Binary Alloy Systems.* Diffusion Foundations, 2015. **4**(1): p. 25.

23. Smigelkas, A.D., Kirkendall, E.O, *Zinc Diffusion in Alpha Brass.* Transactions of AIME, 1947. **171**: p. pp. 130-142.

24. Stephenson, G.B., *Overview no. 75: Deformation during interdiffusion.* Acta Metallurgica, 1988. **36**: p. 2663-2683.

25. Daruka, I., et al., *Diffusion-induced bending of thin sheet couples: Theory and experiments in Ti-Zr system.* Acta Materialia, 1996. **44**: p. 4981-4993.

26. Yin, Y., et al., *Formation of Hollow Nanocrystals Through the Nanoscale Kirkendall Effect.* Science, 2004. **304**(5671): p. 711-714.

27. He, Y.H., et al., *Fabrication of Ti-Al Micro/ Nanometer-Sized Porous Alloys through the Kirkendall Effect.* Advanced Materials, 2007. **19**(16): p. 2102.

28. Onsager, L., *Reciprocal relations in irreversible processes. I.* Physical review, 1931. **37**(4): p. 405.

29. Allnatt, A.R. and A.B. Lidiard, *Atomic transport in solids*. 1993: Cambridge [England] ; New York : Cambridge University Press, 1993.

30. Balluffi, R.W., et al., *Kinetics of materials*. 2005, Hoboken, N.J. : J. Wiley & Sons, 2005.

31. Brady, J.B., *Reference frames and diffusion coefficients*. American Journal of Science, 1975. **275**: p. 954-983.

32. Boltzmann, L., Weid. Ann., 1894. **Vol. 53**: p. pp.959.

33. Matano, C., Jpn. J. Phys., 1933. **Vol. 8** p. pp.109.

34. Kirkwood, J.G., et al., *Flow Equations and Frames of Reference for Isothermal Diffusion in Liquids.* Journal of Chemical Physics, 1960. **33**(5): p. 1505.

35. Heumann, T. and K. Grundhoff, *Diffusion and Kirkendall Effect in the Cu-Ni System.* Z. Metallkunde, 1972. **63**(4): p. 173-180.

36. Wojnar, L., *Image analysis : applications in materials engineering*. CRC series in materials science and technology. 1999: Boca Raton, FL : CRC Press, c1999.

37. Liu, D., et al., *Ternary diffusion in Cu-rich fcc Cu–Al–Si alloys at 1073 K.* Journal of Alloys and Compounds, 2013. **566**: p. 156-163.

38. Trønsdal, G.O. and H. Sørum, *Interdiffusion in Cu-Ni, Co-Ni, and Co-Cu.* Physica Status Solidi (B), 1964. **4**(3): p. 493.

39. Hayashi, E., Y. Kurokawa, and Y. Fukai, *Hydrogen-induced enhancement of interdiffusion in Cu-Ni diffusion couples*. 1998. p. 5588-5590.

40. Askill, J., *Tracer Diffusion Data for Metals, Alloys and Simple Oxides*. 1970, Berlin: Springer.

41. Zhao, J., et al., *Directional electromigration-enhanced interdiffususion in the Cu–Ni system.* Journal of Applied Physics, 2007. **102**(11): p. 114902.

42. Monma, K., H. Suto, and H. Oikawa, *Diffusion of Ni63 and Cu64 in Nickel-Copper Alloys (On the Relation between High-Temperature Creep and Diffusion in Nickel Base Solid Solutions. II).* Vol. 28. 1964. 192-196.

43. E.A. Smirnov, L.I.I., and E.A. Abranyan, Izv. Akad. Nauk, *Experimental study of self-diffusion in copper.* SSSR Metal., 1967. **168**.

44. M.S. Anand, S.P.M., and R.P. Agarwala,, *Diffusion of Copper in Nickel and Aluminum.* J. Appl. Phys., 1965. **36**(12): p. 3860-3862.

45. Wang, J., et al., *Assessment of diffusion mobilities in FCC Cu–Ni alloys.* Calphad, 2008. **32**(1): p. 94-100.

46. Tsai, M.-H. and J.-W. Yeh, *High-Entropy Alloys: A Critical Review*. 2014. p. 107-123.